ATOTA – A VERY PROMISING GREEN FLUOROPHORE

By

HUNG THE DOAN

Bachelor of Science, 2013

Texas Christian University

Fort Worth, Texas

Submitted to the Graduate Faculty of the

College of Science and Engineering

Texas Christian University

in partial fulfillment of the requirements

for the degree of

Master of Science

December 2016

ACKNOWLEDGEMENTS

First of all, I would like to thank my advisor, Dr. Zygmunt Gryczynski. He has not only taken me into the field of wonderful colors and excitements of fluorescence, but he has also guided me throughout the years with concepts, ideas, projects, critiques and sometimes shoulder to shoulder building instrument pieces. He has taught me how to think, how to adapt to the environment and how to improvise when necessary. He has also introduced me to many great scientists around the world, to many people in different fields with hopes that one day I will be able to communicate and work in collaboration with them. I am grateful for everything he did that pushes me forward.

I would also like to thank Dr. Badri Maliwal for being the best mentor I could have asked for during my research at TCU. I also want to thank Dr. Sangram Raut, Dr. Joseph Kimball, and Dr. Sebastian Requena for their help and support as my good friends and lab partners in the last three years. My research time at TCU would not have been as interesting as it is and will be without them.

Lastly, I would like to thank my family and friends, and of course, the most important people that are the reason I am here today, my parents Hieu Doan and Phuong Huyen for their unconditional support and believe in me.

TABLE OF CONTENTS

LIST OF FIGURES

LIST OF TABLES

Chapter 1 Introduction

Over the past few decades, fluorescence detection has become an indispensable technology in many major fields such as chemistry, biology, and recently medicine. Nowadays, fluorescence-based detection plays a prominent role in genomics, cellular imaging, as well as biomedical diagnostics. Although the fluorescence-based method can, under the favorable conditions, detect a single molecule, there is still an ongoing urgent need to create improved and optimized fluorescent probes. In general, an ideal fluorophore for biomedical research will have a small size, high brightness, be photostable, and have a fluorescence lifetime that suits a particular application.

In 2013, we discovered that acridine orange (AO) accumulates inside the mucin granules and forms aggregate with a distinctive red-shifted emission and a ten times increase in the fluorescence lifetime[1]. We successfully utilized AO aggregation to study mucin dynamics in lung epithelial cell using FLIM microscopy, a technique that produces images at cellular level based on the fluorescence lifetimes from a fluorescence sample[1]. However, low extinction coefficient and poor quantum yield of AO are the drawbacks that suffocate the detection speed and limit and put us on a quest of finding a better fluorophore.

In 1998, Laursen *et al*[2] reported the synthesis of a novel highly symmetrical derivative of the triangulenium dyes called ATOTA with very high extinction coefficient and quantum yield. Furthermore, ATOTA is a hydrophobic molecule (solubility less than 20 nM) and forms aggregates which induce a blue-shift in the absorption and a red-shifted emission with ten-fold longer fluorescence lifetime as compared to the monomer[3]. We expect ATOTA to be a very good fluorophore that can overcome the downsides of AO in studying mucus secretion, the first in-line

defense mechanism in human against pathogens and viruses encounters, and exhibit superior performance in cells and tissues.

To fully utilize the potential of ATOTA in the cellular study, we first need to characterize its fundamental spectroscopic properties, many of which may be affected by particular biological conditions. For example, cells with different specialized functions exhibit different polarities. Since ATOTA is a positively charged fluorophore, its fluorescence properties are expected to depend on the interaction with the counter-ion PF_6^- in various polarity environments. It is critical to understand the effect of polarity on ATOTA's fluorescence properties. Therefore, we propose the studies of absorption and fluorescence properties of ATOTA in different polarity environments.

Numbers of the microscopic techniques such as FLIM involve polarization light that interacts with the fluorophore, which has unique transition moments within the molecular structure. The second part of this feasibility study will focus on investigating the transition moment's orientation of ATOTA using linear dichroism and fluorescence anisotropy techniques. The result will help to understand the possible existing and the alignment of the underlying transition moments within the fluorophore's molecular frame.

To utilize ATOTA for mucus secretion study using FLIM microscopy, we would need to understand the correlation between aggregation and the concentration of ATOTA. Therefore, we will first investigate the fluorescence properties of the ATOTA's aggregate in aqueous solution by monitoring its fluorescence as a function of concentration. Fluorescence lifetime is a fundamental property of each particular fluorophore, which can be affected by the process of aggregation. Knowing the fact that ATOTA changes its lifetime upon forming aggregates, we will conduct

time-resolved fluorescence studies to classify the fluorescence lifetime of ATOTA's monomeric and aggregated forms.

Lastly, the combination of ATOTA's hydrophobicity and the potential to form aggregates in non-polar environments make ATOTA an attractive membrane probe due to the affinity between the hydrophobic ATOTA and the non-polar lipid membrane. We address this speculation by characterizing ATOTA fluorescence properties in DMPC –a frequently used lipid bilayer model to mimic the cellular membrane environment.

The results of these studies complimented by the high extinction coefficient and outstanding quantum yield as compared to all currently available organic green dyes may render ATOTA as a very attractive probe for numbers of biological application. Aggregation formation propensity of ATOTA and similarity in spectroscopic properties to AO with exceeding quantum yield also suggests that ATOTA may benefit biophysicists in studying cellular membranes and mucin granules secretion in many respiratory diseases such as cystic fibrosis.

Chapter 2 Basics of fluorescence

Fluorescence is the emission of light by an atom or molecule after a finite duration of time, subsequent to the absorption of electromagnetic (EM) radiation[5]. Specifically, the emitted light arises due to the transition of the excited species/molecules from its first excited electronic state (S_1) to the ground level (S_0). The emitted radiation typically has a longer wavelength (i.e., lower energy) when compared to that of the excitation light. The inherent wavelength difference between the absorbed light and emitted light, called Stokes' shift, allows for very high detection sensitivity. Indeed, fluorescence detection is considered the most sensitive technology that is available today, capable of detecting single molecules. This incredible sensitivity, achievable with harmless radiation (visible and near-IR light), has many potential applications in biological cellular and tissue imaging, environmental studies, as well as in chemistry. Fluorescence is now the leading technology for studying numerous biological processes such as protein–protein interactions, ligand binding, membrane localization, and biomolecular transport *in vitro* (cells in culture) and *in vivo* (tissue and live animals).

2.1 Light absorption

The first process associated with the transition from S_0 to S_n is called the absorption of light. The absorption of light by a molecule depends on the type of the organic molecule, solvent, and other factors. Figure 1 conceptually illustrates the process of absorption by an ensemble of molecules[1]. Each molecule is treated as a semi-transparent disk with an absorption cross section area σ, defined as the effective area of the molecule through which a photon needs to traverse to be absorbed.

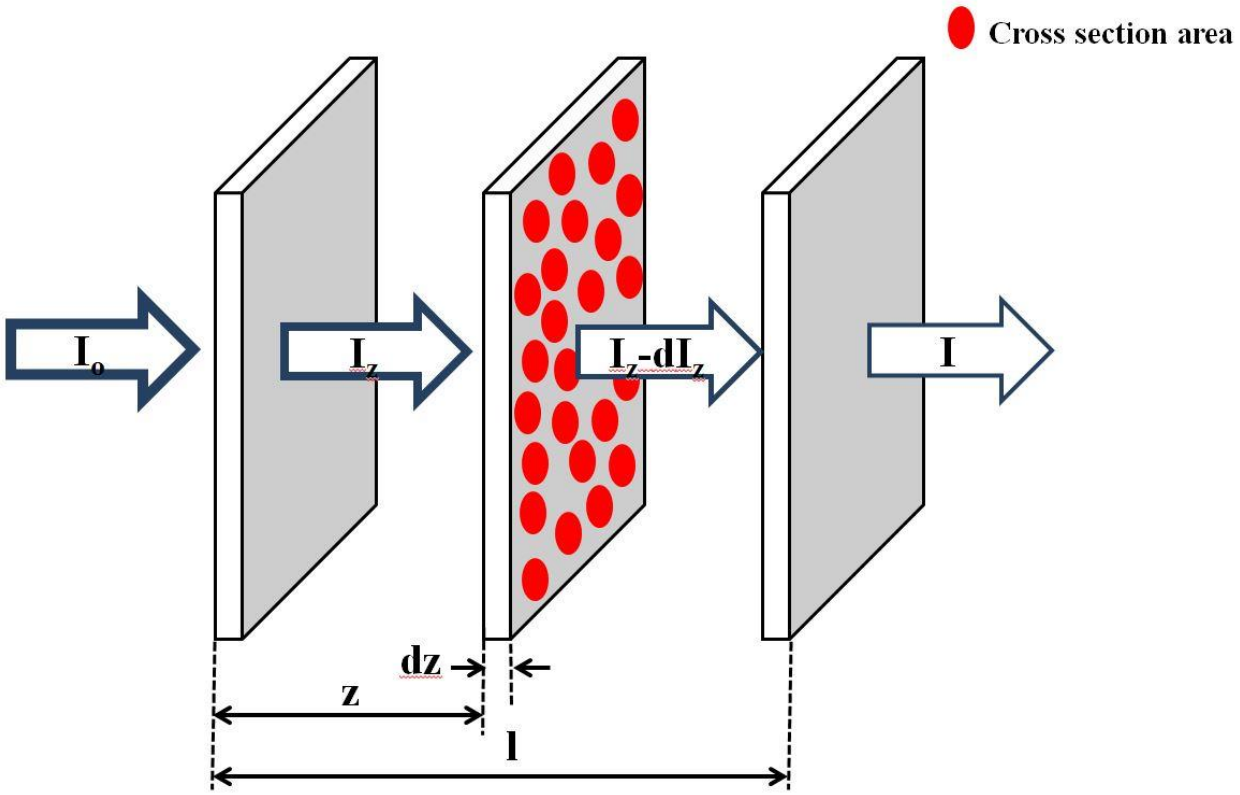

Figure 1: Molecules absorbing light with a defined cross-section area

For a thickness dz of the sample with a total thickness *l*, and total area *S*, $\sigma * N * S * dz$ is the total non-transparent area of the sample, where *N* is the number of molecules per cm^3. The component $(\sigma * N * S * dz)/S$ represents the fraction of absorbed photons traveling through the surface area *S*.

Let's call I_z is the intensity of incoming light that passing through the first layer, and entering the wedge of thickness *dz*. The derivative of this, dI_z, is the intensity absorbed by the wedge.

$$\frac{dI_z}{I_z} = -\sigma * N * dz \qquad (1)$$

Integrating and taking natural logarithm of both sides of Eq.1 gives

$$ln\left(\frac{I}{I_0}\right) = -\sigma * N * l \tag{2}$$

In spectroscopic measurements, it is common to use the ratio of the transmitted light intensity I and the incident light intensity I_0. This ratio is called the "transmittance" T:

$$T = \frac{I}{I_0} \tag{3}$$

For the purpose of simplicity, the cross–section area σ and the number of molecule N can be substituted by the molar extinction coefficient ε and the molar concentration c (mol/l) respectively. Using $N = \frac{c*N_a}{1000}$ (N_a is the Avogadro's constant) and defining $= \frac{\sigma*N_a}{1000*ln(10)}$, Eq.2 can be simplified

$$log\left(\frac{I}{I_0}\right) = -\varepsilon * c * l \quad \text{and} \quad I = I_0 * 10^{-\varepsilon*c*l} \tag{4}$$

Eq. 4 is frequently called the Beer-Lambert law that describes the attenuation of light as it travels through the absorbing medium. The exponent factor defines the absorbance: $Abs = \boldsymbol{\varepsilon} * \boldsymbol{c} * \boldsymbol{l}$. The absorbance depends on the decadic molar extinction coefficient ε of the fluorophore, the molar concentration c of the fluorophore, and the thickness of the sample, $\boldsymbol{l}$, measured in centimeters.

2.2 The Perrin-Jablonski diagram

The interaction of light and a molecule can be illustrated by the Perrin-Jablonski diagram[6] (Figure 2), which represents the electronic states of a molecule and the possible processes that are allowed.

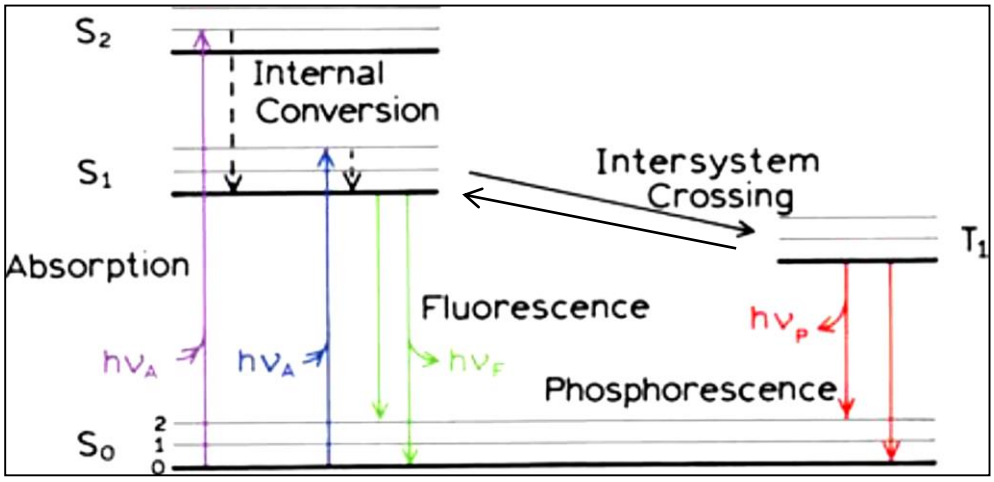

Figure 2: Perrin-Jablonski diagram

In Figure 2, the singlet ground state, the first and second electronic states are represented by S_0, S_1, and S_2 (thick horizontal lines) respectively. Each of these states contains many vibrational energy levels, denoted as 0, 1, 2… (thin horizontal lines). Each vibrational energy level is associated with a quantized amount of energy due to different vibration modes of the molecule. The transitions from the ground states to a higher electronic energy level are represented by the vertical arrows (purple and blue), which illustrate the process of light absorption. The absorption of a photon by a fluorophore is a quick transition (~10^{-15} s, the time needed for a photon to travel a single wavelength) that excites the fluorophore to one of the higher vibrational levels of any allowed excited state. With a few rare exceptions, excited fluorophores quickly relax to the lowest vibrational level of the first excited state, S_1. This process is called "internal conversion" that typically occurs within 10^{-12} s or less. A fluorophore may stay in S_1 for a finite duration of

time, in the realm of 10^{-8} s before returning to one of the vibrational levels of the ground state, which then again quickly reaches thermal equilibrium. The transition from S_1 to S_0 is an allowed transition. The returning to the ground state in a single step with an emission of a photon of an energy corresponding to the difference of energy between the two electronic states is called radiative decay. It is also possible for the molecule to return to the ground state without emission of a photon, where the energy is dissipated as thermal energy/heat. This process is referred to the non-radiative decay. The rates of these two processes are known as the radiative rate, denoted as Γ, and the non-radiative rate, indicated as k_{nr}, respectively.

In some cases, the excited fluorophore in the S_1 state can also go through a spin conversion to a triplet state, denoted as T_1. The transition of S_1 to T_1 is called "intersystem crossing." The transitions from T_1 to the ground state are forbidden. Therefore, the rate constant for emission from T_1 is several orders of magnitude smaller than those for fluorescence. This phenomenon is termed as phosphorescence[7].

2.3 Fluorescence

The radiative transition from S_1 to S_0 after a finite duration of time subsequent to the absorption is called the fluorescence. This phenomenon displays many characteristics.

First, the energy of the emitted photon is typically less than that of the absorbed one (fluorescence occurs at lower energies or longer wavelengths). This wavelength shift between the absorption and fluorescence maxima is called the "Stoke's shift" as shown in Figure 3.

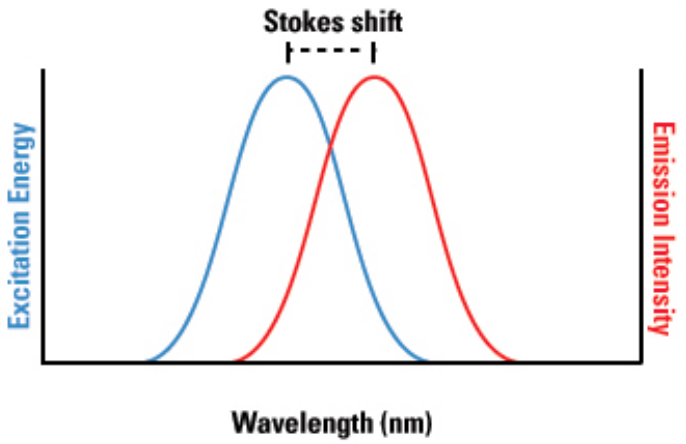

Figure 3: The Stoke's shift

One common source of the Stokes' shift is the rapid return of the excited fluorophores to the lowest vibrational energy level of S_1. Also, when returning to the ground state, instead of going to the lowest vibrational ground state energy level directly, the fluorophore ends up at a higher energy vibrational level of the ground state, resulting in a further loss of the excess vibrational energy by thermalization. Furthermore, the Stokes' shift can be caused by the nature of the solvents, excited-state reactions, and complex formation.

The second characteristic of fluorescence is the fact that the emission spectra are independent of the excitation wavelength; the only difference can be in the intensity of the emission. This excitation independence is referred to as Kasha's rule[8]. In some cases, the emission spectrum obeys the mirror-image of the absorption spectrum. For most fluorophores, emission is the mirror image of the S_0 to S_1 absorption, not the total absorption spectrum covering the transitions to higher energy states. This symmetry is the result of the similar distribution of the vibrational energy levels of S_0 and S_1. The exception to the mirror-image rule happens when a fluorophore changes its conformation or forms complexes in the excited state.

2.3.1 Fluorophores

Fluorescence technologies are widely used nowadays in many biomedical applications due to the sensitivity and versatility of fluorescent probes. A large selection of fluorophores today provides outstanding flexibility, variation, and performance for many research applications. Fluorophores can be divided into two categories: inorganic and organic dyes. Inorganic dyes include lanthanides such as Terbium and Europium, metal-ligand complexes (MCL), quantum dots, fluorescent nanodiamonds, and metal nanoclusters. On the other hand, organic dyes involve natural, synthetic and biological fluorophores. The following is a brief overview of the natural and synthetic organic fluorophores.

Many organic fluorophores occur in nature. They fulfill a variety of physiological functions by interacting with the proteins surrounding them[9,10]. Figure 4 shows the structures of porphyrin, retinal, and carotene as examples of the naturally occurring fluorophores. Light harvesting molecules, such as porphyrins and carotenes, are among the most important naturally occurring fluorophores in photosynthetic systems.

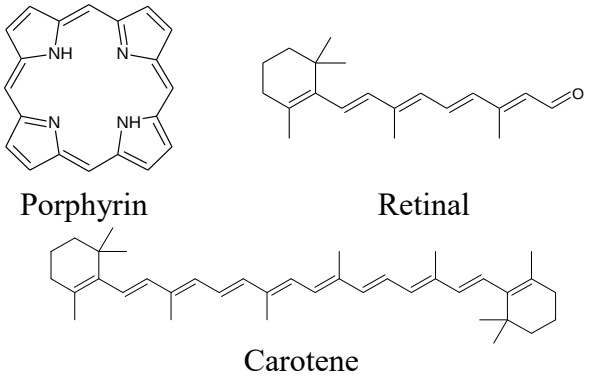

Figure 4: Natural organic fluorophores

Most of the naturally occurring fluorophores, such as the ones shown in Figure 4**,** are chemically neutral. However, the synthetic fluorophores can be either neutral or charged. Some examples of charge carrying fluorophores are shown in Figure 5**.**

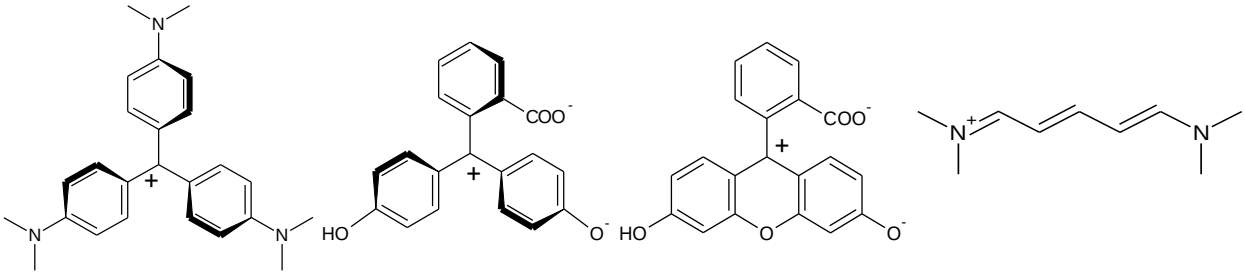

Crystal violet Phenolphthalein Fluorescein A Cyanine

Figure 5: A selection of typical synthetic charged organic fluorophores

The organic fluorophores can be further divided into categories by determining the structure units, usually called the chromophoric units, of each fluorophore. The most fundamental chromophoric unit of a fluorophore is the double bond (the π-electron system), which plays the role of a dipole antenna in interacting with the electric field of light. A "polyene dye" is a fluorophore that is made up entirely of carbon double-bonds, with an even number of atoms in its conjugated system. On the other hand, "polymethine dye" is a fluorophore with an uneven number of unsaturated carbon atoms in its conjugated system. Polyene dyes are all charge neutral while polymethine dyes are all charged.

The emission of fluorescence occurs quite often in polythethine dyes with large locked conjugated π-systems, for example, pyrene and anthracene[11,12]. We can further divide polymethine dyes into several classes. Figure 6 shows the basic structure of the four commercially available reactive forms of polymethine dyes, including xanthenium, cyanine, squarine, and BODIPY.

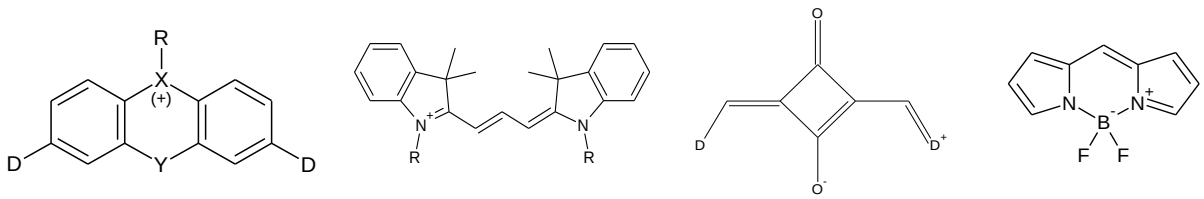

(a)Xanthenium (b)Cyanine (c)Squaraine (d)BODIPY

Figure 6: The commercially available in reactive form fluorophores

In Figure 6 from left to right, the first class is the xanthenium dyes (Fig. 6a). The substituent labeled as "D" can be oxygen or a nitrogen atom, while "X" and "Y" can be carbon, oxygen, nitrogen or sulfur. The classic examples of the xanthenium dyes are fluorescein, rhodamine, Alexa dyes, and dylights dyes. The second class is the cyanine dyes with various ring structures (Fig. 6b). The most distinguished members of the cyanine dyes class are the Cy-dyes family, for example, the Cy5 fluorophore which was the first commercially available amine reactive near infrared (NIR) dye. The third class consists of squaraine dyes, where "D" can be any ring structure with heteroatoms (Fig. 6c). Squaraine dyes are well-known for their high two-photon cross-section area. Also, upon excitation, squaraine dyes can also release a singlet oxygen agent, which is the key element in photodynamic therapy[13]. The last dye class is BODIPY (Fig. 6d). The alkyl-substitute derivatives of BODIPY have a green, fluorescein-like fluorescence. However, adding substituents that comprise additional conjugates to the core structure can shift both absorption and emission spectra of BODIPY to a longer wavelength. Currently, it is possible to acquire the reactive forms of BODIPY derivatives with emission maxima approaching 800 nm.

For every newly synthesized fluorophore, an in-depth spectroscopic investigation is the first step in bringing the dye into biological applications and directing further synthetic approaches.

2.3.2 Fluorescence Quantum Yield (QY)

The fluorescence quantum yield is a fundamental characteristic of a fluorophore. The QY is defined as the number of photons being emitted relative to the number of photons being absorbed.

$$QY = \frac{\#photons\ emitted}{\#photons\ absorbed} \tag{5}$$

The QY can also be described by the ratio of the radiative rate (Γ) to the sum of all the rates ($\Gamma + k_{nr}$).

$$\mathrm{QY} = \frac{\Gamma}{\Gamma + \mathrm{k_{nr}}} \tag{6}$$

If the radiative rate is much larger than non-radiative ($\Gamma >> k_{nr}$) the QY approaches 1 and if the $\Gamma << k_{nr}$ the QY drops to 0.

2.3.3 Fluorescence Lifetime (τ)

Fluorescence lifetime is the average time a fluorophore stays in the excited state S_1 before returning to the ground state. Typically, fluorescence experiments involve the excitation of a vast number of molecules and the emission of many photons. Therefore, it is practical to look at the deactivation of the excited state as a statistical process. Excited molecules decay from the excited state randomly, leading to an exponential decay of the population of excited molecules.

Mathematically, the fluorescence lifetime can be interpreted as follows: suppose *N* molecules are excited with a delta function pulse of light. After the excitation, the excited population of molecules decays with the rate $\Gamma + k_{nr}$.

$$\frac{dN(t)}{dt} = -(\Gamma + k_{nr})N(t) \quad (7)$$

Here *N(t)* is the number of excited molecules at time t. The emission of each molecule happens randomly with a constant probability. The solution of Eq. 7 gives us

$$N(t) = N_0 e^{-t(\Gamma + k_{nr})} \quad (8)$$

At time $t = \tau = (\Gamma + k_{nr})^{-1}$, the number of molecules remaining in the excited state will be $N = N_0 e^{-1} = 0.368 N_0$ *or* 36.8% of N_0. The time τ is called the fluorescence lifetime.

Since the fluorescence intensity is directly proportional to the number of excited molecules, the time-dependent fluorescence intensity can also be described as an exponential decay:

$$I(t) = I_0 e^{-t/\tau} \quad (9)$$

2.3.3.1 Time Correlated Single Photon counting (TCSPC)[14]

Time Correlated Single Photon Counting (TCSPC) is a well-established method that uses pulsed light sources (preferentially with a high repetition rate) and accumulates a large number of photon events. In principle, TCSPC detects the arrival times of the first photon reaching the detector after each excitation pulse. The principle of TCSPC can be illustrated by examining the instrument schematic in Figure 7.

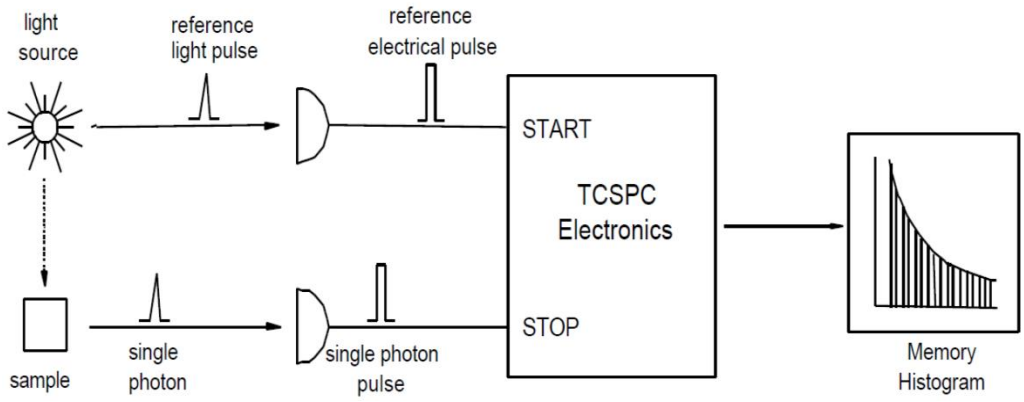

Figure 7: Schematic of TCSPS instrumental

A sample is excited by a pulsed laser light source with a high repetition rate (typically MHz). One can look at the TCSPC electronic as a fast stopwatch with two inputs. An excitation pulse excites the sample and starts the clock; the photon detection signal stops the clock. The memory histogram represents the number of counted photons (events) for each channel as a function of time. With a high repetition rate of excitation light source, millions of start-stop sequences can be measured in a short period (seconds).

Detectors and TCSPC electronics have a dead time (the time it takes to relax and be ready for the next photon detection, usually of 25 to 90 ns. It is necessary to have a low count rate so that the probability of detecting two or more photons in one signal period (the time between stimulating pulses) is negligibly small. The detection rate usually is 1% photons per single excitation period (1 photon detected per 100 pulses). Multiple photons arriving in a single cycle would not be detected and will not be accounted for in the statistics. Higher detection rate (usually more than 5% will lead to higher probability of detecting only the earlier photons and this phenomenon is termed the "pulse pile-up effect" that causes the apparent shortening of the measured fluorescence lifetimes. A low counting rate assures that the detector has the same probability of detecting a photon in anytime at every excitation cycle.

2.3.3.2 TCSPC Data Analysis – Convolution integral (Fitting)

In practice, the excitation pulse is not a δ-function. A real excitation pulse has a width of picoseconds to nanoseconds. The measured intensity decay is, therefore, convoluted with the lamp function (Figure 8). To resolve this convolution, the excitation pulse can be considered to be a series of different amplitudes of δ-functions. Each of these δ-functions corresponds to an impulse response from the sample with the signal proportional to the intensity of the corresponding excitation pulse. The measured function will be the sum of all exponential decays, each of different amplitudes at different times.

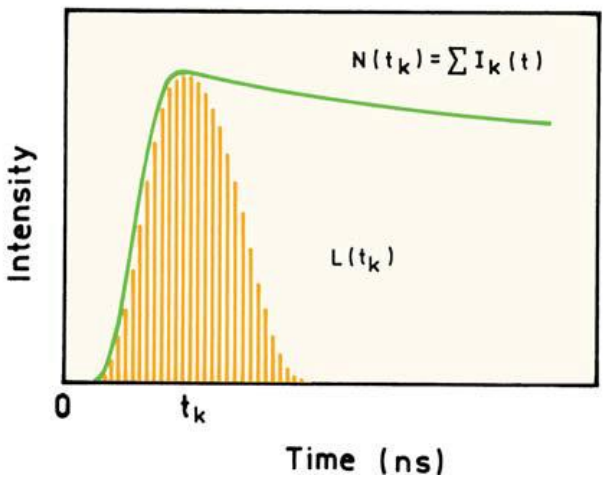

Figure 8: Convolution of an impulse response function *I(t)* with a lamp profile $L(t_k)$ to yield the measured data $N(t_k)$

Assuming each δ-function excites a sample at time t_k [6], the concept of convolution can be illustrated as

$$I_k(t) = L(t_k).I(t - t_k).\Delta t \qquad (t > t_k) \qquad (10)$$

The term $t - t_k$ represents the intensity decay due to the impulse response started at time $t = t_k$. There is no emission before the excitation when $t < t_k$. The measured decay *N(tₖ)* is the sum of the impulse responses created by all the individual *δ*-function excitation pulses that happen until t_k.

$$N(t_k) = \sum_{t=0}^{t=t_k} L(t_k).I(t - t_k).\Delta t \tag{11}$$

For an infinitely small *Δt*, Eq. 11 can be rewritten as an integral.

$$N(t) = \int_0^t L(t').I(t - t').dt' \tag{12}$$

The measured intensity at time *t* is given by the sum of the intensities expected for all the *δ*-function excitation pulses that occur during the time *t*. Notice that the sample will generate new intensity decays as long as there is nonzero intensity in *L(tₖ)*. Replacing $t' = t - \mu$, the convolution integral can be expressed as

$$N(t) = \int_0^t L(t - \mu).I(\mu).d\mu \tag{13}$$

Recall the intensity decay at time *t*

$$I(t) = I_0.\exp(\frac{-\mathrm{t}}{\Gamma + \mathrm{k_{nr}}}) \tag{14}$$

Thus, *N(t)* is rewritten as

$$N(t) = \int_0^t L(t - \mu).I_0.e^{-\frac{t}{\tau}}.dt \tag{15}$$

The obtained signal is a convolution of the lamp function $L(t-\mu)$ and the real intensity decay $I_0.e^{-\frac{t}{\tau}}$. The actual intensity decay can be achieved after the deconvolution. The intensity decay represents the distribution of the number of photons at a given arrival times. An exponential function is used to fit the collected data.

The most commonly used method to deconvolute the real intensity decay is nonlinear least-square analysis[15-17]. In any least square analysis, we start with a model that is assumed to describe the data. The goal is to determine the parameters that provide the best fitting between the measured data set $N^{ob}(t)$ and the calculated decay $N^{cal}(t)$. To achieve those parameters, we must minimize the goodness-of-fit parameter χ^2 [7].

$$\chi^2 = \sum_{i=1}^{n} \left[\frac{N^{ob}(t_i) - N^{cal}(t_i)}{N^{ob}(t_i)} \right]^2 \qquad (16)$$

2.3.2 Fluorescence polarization/anisotropy

Upon excitation with polarized light, molecules in a sample whose transition dipole moments are oriented parallel to the electric field vector *E* of the excitation light will be preferentially excited. This effect is referred to as photo-selection, which results in polarized fluorescence emission of the sample. The origin of this phenomena is due to the existence of the transition dipole moments for absorption and emission which have fixed orientations within a molecular frame. Consider an *XYZ* coordinate system in a simple fluorescence anisotropy measurement with a fluorophore solution at the origin as in Figure 9

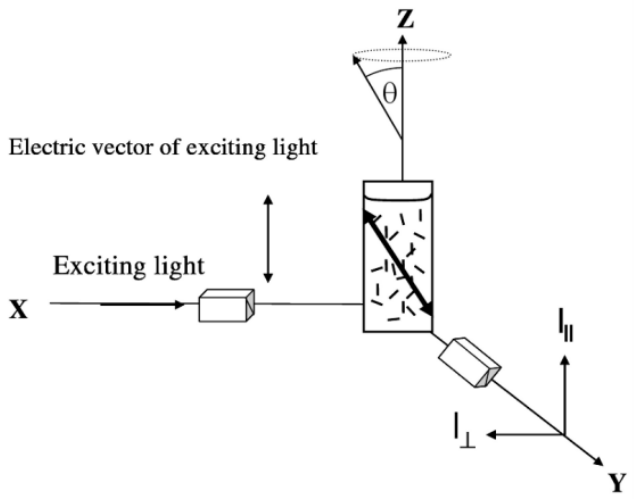

Figure 9: Schematic diagram for measurement of fluorescence anisotropy

Let's assume the transition moment of the molecule, also known as the electric dipole moment that associates with the transition between different energy levels, forms an angle θ with the *Z*-axis. The interaction of the transition moment with the electric field of amplitude E that has direction *Z* is proportional to $cos\,\theta$. Since the intensity of the electromagnetic radiation is proportional to the square of its amplitude, the probability for a transition moment to interact with the electromagnetic radiation of a given intensity is proportional to $cos^2\,\theta$.

In this system, the excitation light propagates along the X-axis and is polarized parallel to the *Z*-axis. The fluorophores absorb the excitation light, and their fluorescence emission is observed along the *Y*-axis through a polarizer which can be oriented parallel or perpendicular relative to the *Z*-axis. The two corresponding observed intensities are $I_{\|}$ (parallel) and $I_{\perp}$(perpendicular). The polarization of the emission light is defined as:

$$P = \frac{I_{\|} - I_{\perp}}{I_{\|} + I_{\perp}} \tag{17}$$

Another more general term in the context of polarized light is the emission anisotropy. Emission anisotropy for an isotropic system with cylindrical symmetry, can be defined as

$$r = \frac{I_{\parallel} - I_{\perp}}{I_{\parallel} + 2I_{\perp}} \tag{18}$$

Theoretically, the limit of polarization for the isotropic system is -0.33 to 0.5 and -0.2 to 0.4 for anisotropy[7]. Those limiting values can only be reached in systems that satisfy two conditions. First, the fluorophore must have co-linear absorption and emission transition moments, and second, the system must be completely frozen (no molecular rotation between absorption and emission processes). In the case when the absorption and the emission transition moments form an angle α, the anisotropy of the system is[7]

$$r = 0.4\left(\frac{3\,cos^2\,\alpha - 1}{2}\right) \tag{19}$$

The two extreme values of α are 0° and 90°, which make the limiting anisotropies for a solution of fluorophore +0.4 and -0.2 respectively. At an angle $\alpha = 54.7°$, the system anisotropy is zero.

In a solution where the fluorophores can rotate freely, the observed anisotropy will be affected not only by the limiting anisotropy but also by the extent of rotational diffusion of the molecule before it emits light during the period between absorption and emission. The characteristic lifetime of the rotational diffusion, also called the rotational correlation time (Θ), is defined as the time it takes for the molecule to rotate over an angle of one radian. The rotational correlation time reflects on how fast the molecule rotates and is given by

$$\Theta = \frac{\eta V}{RT} \tag{20}$$

Eq. 20 indicates the dependence of a fluorophore's rotational correlation time on a number of factors such as the molecular volume *V* of the fluorophore (size of the molecule), the viscosity η of the solvent, the temperature *T*, and the gas constant *R*. In the solution, the rotational diffusion of the excited molecules (photoselected molecules) randomizes the orientation of the excited dipoles leading to lowering the measured anisotropy. The smaller the fluorophore, the faster it rotates. Furthermore, when a small fluorophore binds to larger biomolecules, it will rotate slower. As a result, the fluorescence anisotropy can be used advantageously to study the structure of the proteins, the rigidity of probes molecular environments, as well as protein-protein interactions, ligand binding, immunoassay, and live cell imaging.

After pulsed excitation, the photo-selected dipole reorients resulting in time-dependent fluorescence anisotropy. For simplicity, let us assume the fluorophore rotates with a single correlation time Θ. At time $t = 0$, after δ-pulse excitation, the anisotropy decay only depends on the relative orientation of the absorption and emission transition moments and give the so-called the limiting anisotropy r_0 (maximum anisotropy for a given vector configuration of absorption and emission transition moments). The time-dependent fluorescence anisotropy, *r(t)*, can be described using the equation

$$r(t) = r_0 e^{-\frac{t}{\theta}} \tag{21}$$

For spherically symmetrical molecules, the anisotropy decay can be described by a single exponential model. However, this is not always the case. Observation of multiple exponential anisotropy decays implies that the molecule under investigation displays either an asymmetrical geometry or the presence of local motions independent of overall rotation, or both. The time-dependent anisotropy for various correlation times can be described as a multi-exponential decay

$$r(t) = \sum_j r_{0j} e^{-\frac{t}{\theta_j}} \qquad (22)$$

Here θ_j is the individual correlation times, r_{0j} is the fractional anisotropy which decays with the correlation time θ_j, and $\sum_j r_{0j}$ represents the limiting anisotropy in the absence of rotational diffusion at time *t=0*.

2.4 Quenching of Fluorescence – Energy transfer

Fluorescence quenching relates to a variety of molecular interactions, which reduces the fluorescence intensity of a sample. Fluorescence quenching can occur by different mechanisms, involving processes such as excited-state interactions, molecular rearrangements, and ground-state complex formation. The study of fluorescence quenching provides valuable knowledge about the dynamic processes in the solutions. Some of the common mechanisms of fluorescence quenching are the fluorescence resonance energy transfer (FRET), contact quenching (static), and collision quenching (dynamic). Figure 10 illustrates the general mechanisms of each process.

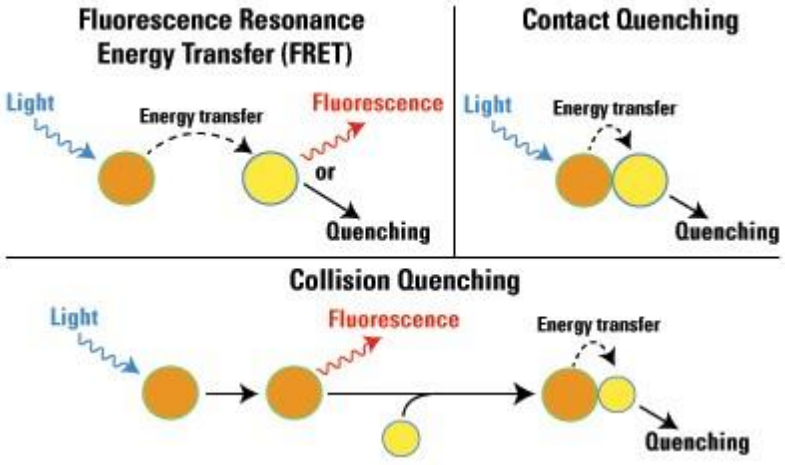

Figure 10: Mechanism of quenching[18]

In contact quenching (static quenching), the fluorophore forms a non-fluorescent complex with a quencher molecule in the ground state. Upon excitation, the direct contact between the two molecules leads to an immediate deactivation of the excited molecule in a non-radiative way, and the energy is dissipated in the form of heat.

Collision quenching (dynamic quenching) occurs when the quencher diffuses and gets in contact with the excited fluorophore and deactivates the excited state in non-radiative processes. The interaction happens during the lifetime of the excited state of the fluorophore. This process will depend on the fluorescence lifetime and the diffusion of the quencher (viscosity).

FRET is a particular case of quenching that occurs in the excited state when there is an overlap distance between the emission spectrum of a fluorophore, called the donor, and the absorption spectrum of another molecule called the acceptor. Upon excitation, the donor, instead of returning to the ground state and emitting a photon, transfers the energy to the nearby acceptor. The acceptor can be nonfluorescent. If the acceptor is another fluorophore, its emission will have a longer wavelength as compared to the donor. FRET happens without an intermediate photon emission from the donor; the donor and acceptor are coupled by dipole-dipole interactions. These interactions happen only up to a certain distance (less than 10 nm). Therefore, FRET can be used for very precise measurements of distances between two interacting molecules (donor and acceptor). If the donor and acceptor are the same molecules with significant overlap between the excitation and emission spectra, the process of transferring energy is called homo-FRET[19].

Chapter 3 Linear Dichroism (LD)

One of the properties of linear transition moments is the fact that a molecule will preferentially absorb light with a plane of polarization parallel to the direction of its transition moment. In other words, when linearly polarized light interacts with a single chromophore, the probability for absorbing a photon will be maximal for transition moment oriented parallel to the electric field of incident light, and for transition moment oriented orthogonally, it will be zero. For an ensemble of oriented (or even only partially oriented) molecules, the absorption of light will depend on the light polarization. If the direction of chromophores orientation is defined as *Z*, the difference in absorption between light polarized parallel to *Z* and light polarized perpendicular to *Z* is called linear dichroism (LD):

$$LD = Abs_{\parallel} - Abs_{\perp} \qquad (23)$$

There are many oriented or partially oriented systems. Among them are crystals, liquid crystals, oriented membranes, stretched polymer films, or even elongated molecules flowing through a capillary may show the partial orientation of long molecular axis. One very convenient approach to align the fluorophores is to embed them into a polymer that can be linearly stretched. Typically, the fluorophore is incorporated into a polymer solution, which in our case is polyvinyl alcohol (PVA). After drying, the PVA film will subsequently immobilize fluorophores randomly in the polymer matrix. Upon stretching the PVA film, the polymer chains align along the stretching direction forcing fluorophores to align long molecular axis along the stretching direction as well. The chromophores orientation directly depends on the stretching ratio $R_s = \frac{a}{b}$. Where, a is the semi-axial major, and b is the minor axis of an ellipsoid deformed from an initial sphere envisioned in the isotropic film[20-22].

In such oriented film, the two absorption components are measured for light polarization parallel (∥) to the stretching direction, $Abs_{\parallel}$, and perpendicular (⊥) to it, $Abs_{\perp}$, and linear dichroism is given by Eq. (23). The dichroism of light absorption can also be presented in the form of the dichroic ratio R_d

$$R_d = \frac{Abs_{\parallel}}{Abs_{\perp}} \tag{24}$$

To describe the orientation of a molecule in a stretched PVA film, we can use three Euler angles (α, β, Υ)[23] as shown in Figure 11**.** These angles correspond to the rotation of the molecule-fixed coordinate system (*x*, *y*, *z*) in related to a fixed coordinate system (*X*, *Y*, *Z*). The orientation axis z can be defined as the direction in the coordinate system, in which the transition moment should be aligned to give the maximum dichroic ratio $R_d = \frac{E_z}{E_y}$, where $E_z(\lambda)$ and $E_y(\lambda)$ represent the absorbance along the *z* and *y*-axes. The direction perpendicular to *z*, which provides the highest dichroic ratio, is defined as *y*. The x-axis is perpendicular to both *y* and *z*.

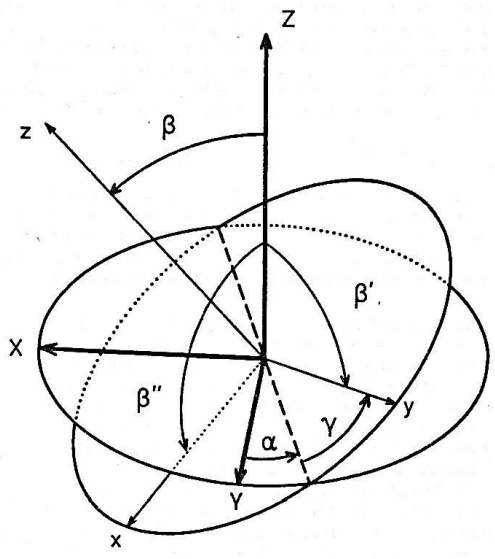

Figure 11: (X, Y, Z) and (x, y, z) coordinate systems and the Euler angles

It is useful to introduce the angles β, β' and β'' between the *Z* axis and the molecular axes *z*, *y* and *x*, respectively. The angle β' and β'' are related to the Euler angle β by

$$cos\beta' = sin\beta sin\Upsilon, \text{ and } cos\beta'' = sin\beta cos\Upsilon \quad (25)$$

It is trivial to show that

$$cos^2\beta + cos^2\beta' + cos^2\beta'' = 1 \quad (26)$$

Many important planar molecules belong to the symmetrical point groups (D_{2h}, C_{2v}), which limit the electronic transition moments to two perpendicular directions in the plane of the molecule with a negligible contribution of the transition along perpendicular to the plane axis (out-of-plane transitions). The first two axes, *z*, and *y* are in-plane (providing the maximum of the dichroic ratio), and *x* is usually out-of-plane. Figure 12 gives an example of a planar aromatic hydrocarbon fitting this description. The x-axis is perpendicular to the molecular planes defined by *y* and *z*.

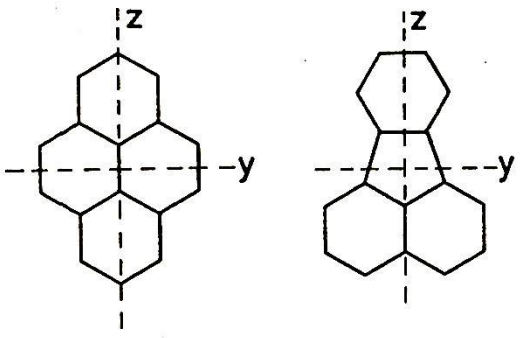

Figure 12: Planar aromatic hydrocarbon with electronic transition moments axes

Introducing the following notations

$$< cos^2\beta >= K_z$$

$$< cos^2\beta' >= K_y \tag{27}$$

$$< cos^2\beta'' >= K_x$$

where $K_x, K_y,$ and K_z are the orientation factors along the *x*, *y*, and *z* axes. From Eq. 26 and Eq. 27, we have

$$K_x + K_y + K_z = 1 \tag{28}$$

The set of *K*'s is linearly dependent. The observed absorbance can be written as

$$\begin{aligned} E_z(\lambda) &= \textstyle\sum_{i=x,y,z} K_i\, A_i(\lambda) \\ E_y(\lambda) &= \sum_{i=x,y,z} \frac{1}{2}(1 - K_i)A_i\,(\lambda) \end{aligned} \tag{29}$$

Or

$$\begin{aligned} E_z(\lambda) &= K_z A_z(\lambda) + K_y A_y(\lambda) + (1 - K_z - K_y)A_x(\lambda) \\ E_y(\lambda) &= \frac{1}{2}[(1 - K_z)A_z(\lambda) + (1 - K_y)A_y(\lambda) + (K_z + K_y)A_x(\lambda)) \end{aligned} \tag{30}$$

Adding two equations in Eq.30 gives:

$$E_z(\lambda) + 2E_y(\lambda) = A_z(\lambda) + A_y(\lambda) + A_x(\lambda) = 3A(\lambda) \tag{31}$$

where $A_z(\lambda)$, $A_y(\lambda)$ and $A_x(\lambda)$ are absorption components polarized along the three axes and $A(\lambda)$ the absorption of an isotropic sample.

One of the most important cases is when $A_x(\lambda) = 0$, for example, the π- π^* transitions in planar molecules. Simplifying Eq. 30 yields

$$E_z(\lambda) = K_z A_z(\lambda) + K_y A_y(\lambda)$$
$$E_y(\lambda) = \frac{1}{2}[(1 - K_z)A_z(\lambda) + (1 - K_y)A_y(\lambda)] \quad (32)$$

Another particular case is that of a "disk-shaped" molecule when $K_z = K_y$. Further simplification of Eq. 32 gives

$$E_z(\lambda) = K_z[A_z(\lambda) + A_y(\lambda)]$$
$$E_y(\lambda) = \frac{1}{2}(1 - K_z)[A_z(\lambda) + A_y(\lambda)] \quad (33)$$

A convenient way of illustrating the orientation of the molecules in an anisotropic medium and the relation between the *K*'s is the orientation triangle, as shown in Figure 13.

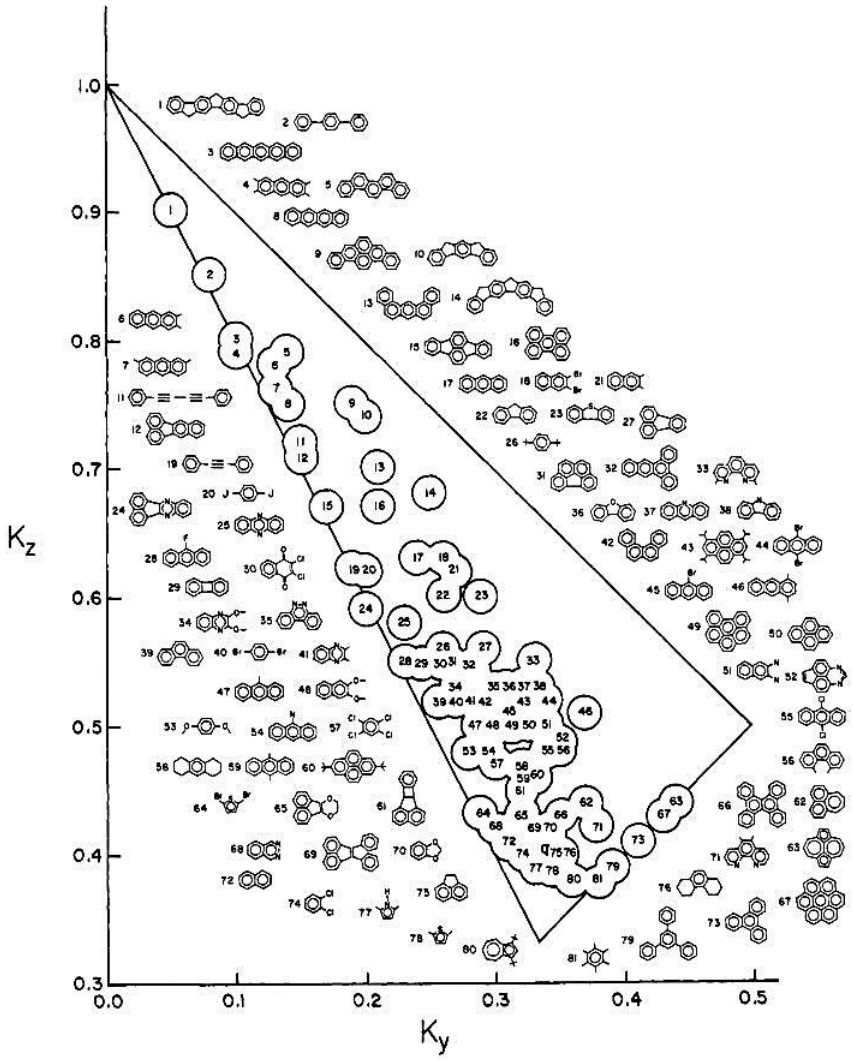

Figure 13: The orientation triangle illustratess the orientation factor along the y and z-axes[24]

For disk-like orientation molecules such as coronene (molecule numbered 67) and triphenylene (molecule number 73)

$$K_y = K_z, \qquad K_x = \frac{(1 - K_z)}{2} \tag{34}$$

For rod-like orientations molecules such as anthracene (molecule numbered 17)

$$K_y = K_x = \frac{1 - K_z}{2} \tag{35}$$

For perfect alignment of molecular plane with stretching direction (top left region),

$$K_y = 1 - K_z, \qquad K_x = 0 \tag{36}$$

Chapter 4 Reviews of ATOTA

In 1964, Martin and Smith[25] followed the speculations about the possibility of making a polyaromatic triangle and successfully synthesized a triangulenium dye with three oxygen bridges, as shown in Figure 14. It is called the trioxatriangulenium dye and makes up a whole new class of fluorophore.

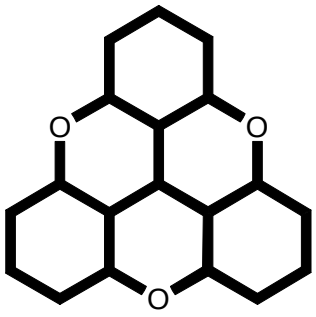

Figure 14: Structure of a trioxatriangulenium dye

The structure of the trioxatriangulenium dye is highly symmetrical. The breakthrough of Martin and Smith gave rise to the successors in producing numbers of extended derivatives of the trioxatriangulenium dye with nitrogen substitutions in the ring system and on the periphery. Figure 15A shows the fundamental modification points (red circles) on the shorthand structures of the trioxatriangulenium dyes and Figure 15B illustrates some key derivatives in this class.

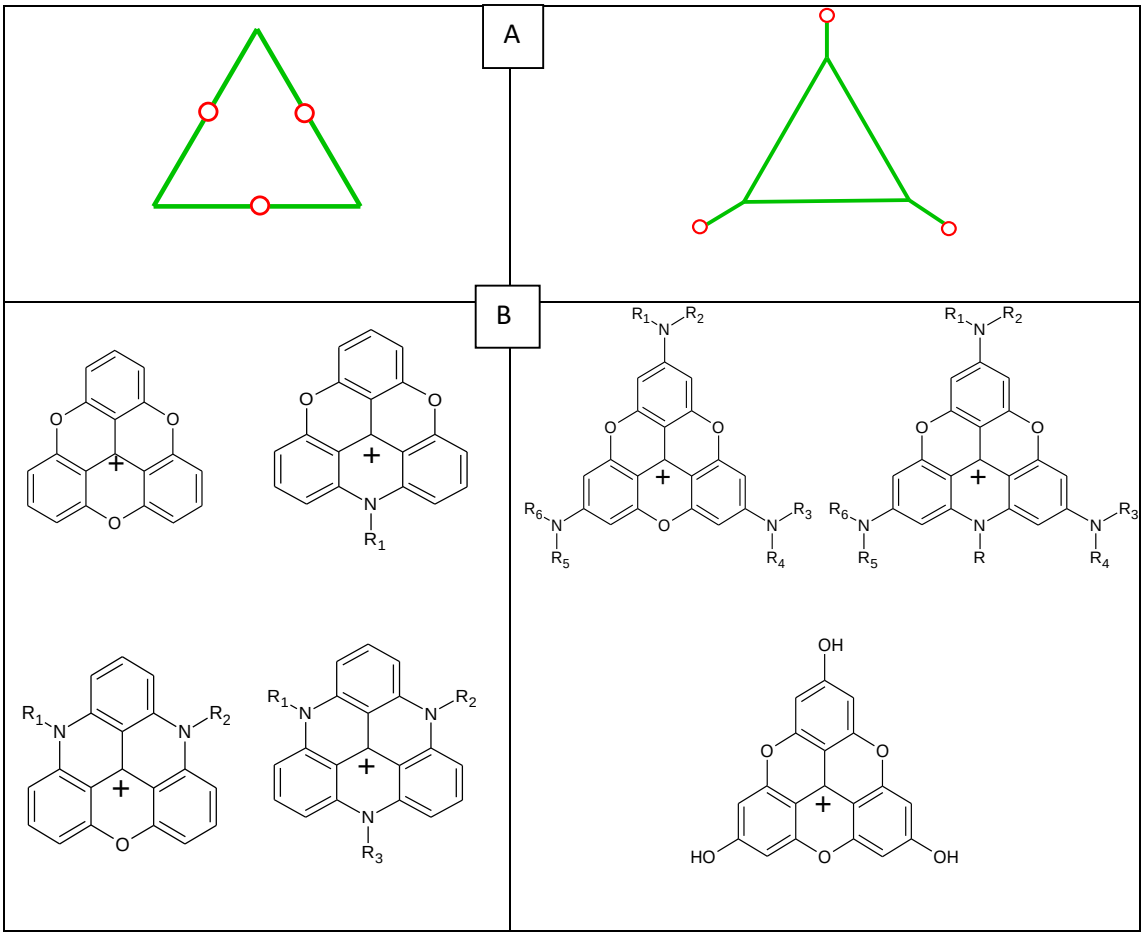

Figure 15: (A) The shorthand structure of trioxatriangulenium dyes. (B) Key derivatives

In 1998, B. W. Laursen[2] and his group introduced an oxa-triangulenium dye named ATOTA$^+$ with very high molar extinction at the common 470 nm-490 nm excitation range in most commercial microscopy systems. ATOTA$^+$ is positively charged at the center carbon and has three peripheral substituted amino groups. The section below summarizes the studies of B. W. Laursen and his group on ATOTA$^+$.

Figure 16 shows the connection in structure between ATOTA$^+$, rhodamine family such as Rh3B$^+$ and triphenylmethane dyes (TMP) such as CV$^+$. The ATOTA$^+$'s structure is planar while CV$^+$ has two phenyl groups twisted out-of-plan and Rh3B$^+$ has one. The twisting of the phenyl groups of TMP dyes out of plane causes a red shift in the absorption, while the introduction of electron

donating substituents in the ortho and para position causes a hypsochromic shift (blue shift) in the absorption[26,27].

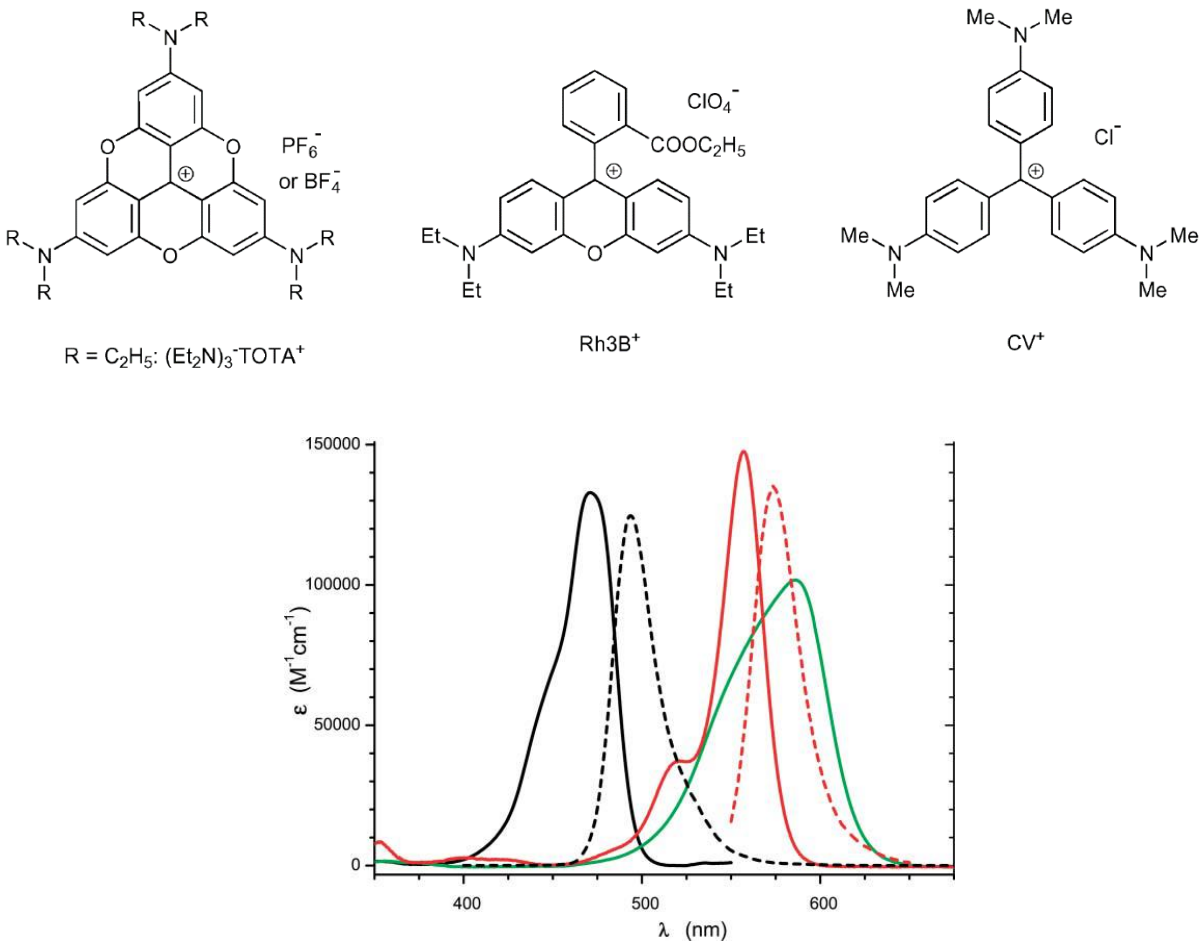

Figure 16: Structures ATOTA$^+$ (black), rhodamine 3B (Rh3B$^+$) (red), and crystal violet (CV$^+$) (green) and their absorption (solid lines) and fluorescence (dashed lines) spectra in CH_2Cl_2

Figure 16 presents the absorption and emission of the planar ATOTA$^+$ (black lines) molecule in dichloromethane which has $\lambda_{max}^{abs} = 471\,nm$ and $\lambda_{max}^{em} = 494\,nm$. Having two out-of-plane phenyl groups, CV$^+$'s absorption (green line) has $\lambda_{max}^{abs} = 598\,nm$ and λ_{max}^{em} (not shown) below

700 nm. $Rh3B^+$ with only one out-of-plane phenyl group has absorption and emission spectra (red lines) in the intermediate of $ATOTA^+$ and CV^+.

Laursen and coworkers found that the binding of different counter-ions modified the absorption of $ATOTA^+$. Figure 17 shows the absorption of $ATOTA^+$ in benzene with four different counter ions: Cl^- (black), BF_4^- (red), PF_6^- (green) and TT^- (blue). The concentration of both $ATOTA^+$ and the counter-ions were 5 μM; these spectra were normalized at the S_1 transition. The presence of counter-ion in highly nonpolar (benzene) resulted in two peaks of similar intensities centered around 450 nm and 500 nm. The peak in dichloromethane, in contrast, was centered at 471 nm (Figure 16).

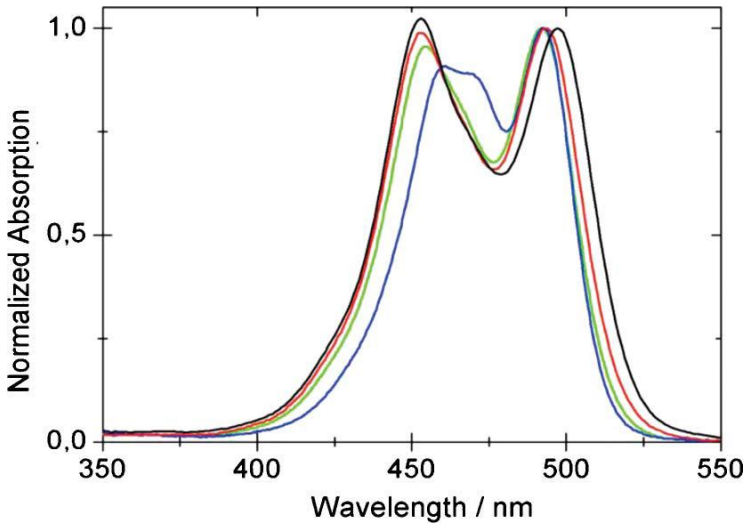

Figure 17: Normalized absorption spectra of $ATOTA^+$ (PF_6^-) in benzene with various counter-ions

Based on their studies on changes in absorption properties of $ATOTA^+$'s in various solvents and lipid bilayer, Bo. W. Laursen *et al*[3] proposed a three states model assigning the characteristic absorption spectra of $ATOTA^+$ (PF_6^-) in solvents as shown in Figure 18. From left to right: solvated ion illustrates the cases when the $ATOTA^+$ and its counter ion are solvated in aqueous solution

while a tight ion pair describes the cases when ATOTA$^+$ and its counter ion are in proximity in the solvent. Two ion pairs form a dimer which can further grow in larger aggregates.

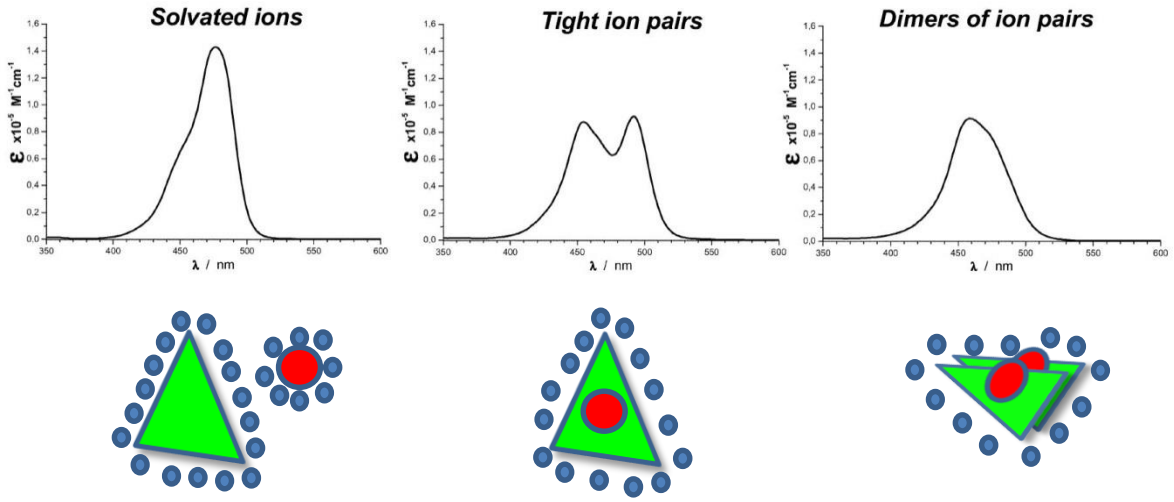

Figure 18: Three-states model of ATOTA$^+$

Laursen' group also synthesized several fatty acid derivatives of ATOTA$^+$ [28]. One such amphiphilic fatty acid derivative sodium 2-didecylamino-6,10-bis(N-methyltaruino)- 4,8,12-trioxatriangulenium (Na-DSA) is shown in Figure 19. They prepared the unilamellar vesicles (without sonication) by mixing powders of this derivative at (5 mol %) and DMPC in aqueous solution and shaking it for 4 hours[29].

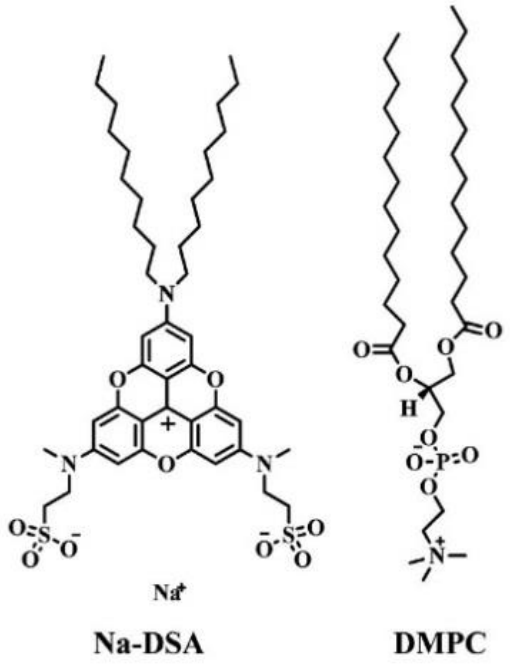

Figure 19: Molecular structure of Na-DSA and DMPC

The absorption of Na-DSA in DMPC (Figure 20) has a peak at 450 nm and a shoulder at around 500 nm. This absorption spectrum is unlike that seen in dichloromethane (471 nm peak) or benzene (two equal intensity peaks at 450 nm and 500 nm). They attributed this 450 nm centered absorption band to the dimer formed by the stacking of Na-DSA. Such stacking was driven by the need to bury a polar triangulenium in the hydrocarbon core of DMPC vesicles and was also helped by the attractive forces between the hydrophobic carbon tails of DMPC and Na-DSA.

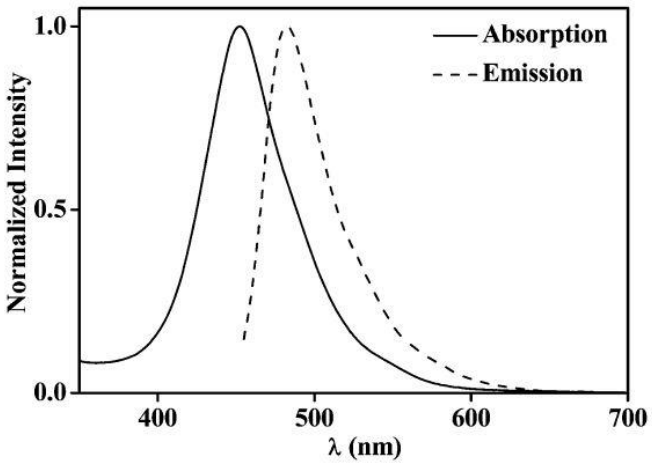

Figure 20: Normalized absorption and emission (excited at 450 nm) spectra of 5% DSA solution

The previous studies of ATOTA gave an insight of the potential of ATOTA as a bright green fluorophore for many biotechnology applications, including cellular imaging (FLIM) and probable cellular membrane and mucin granules secretion studies. The results of my research in the next section will provide an in-depth study of ATOTA for purposes of utilizing ATOTA into biophysical applications. The results include a full characterization of ATOTA's fluorescence properties in different polarity environments, the study of the orientation of ATOTA's transition moments, the study of ATOTA's aggregation, and the preliminary study of ATOTA in a lipid bilayer membrane model.

Chapter 5 Results

5.1 Materials and methods

$ATOTA^+(PF_6^-)$ (shortcut as $ATOTA^+$) was received from Dr. Laursen. The synthesis was described in Laursen *et al*[2]. DMPC was acquired from Avanti Polar Lipids and Polyvinyl alcohol (PVA) powder (molecular weight 130,000 g/mol) from Sigma-Aldrich. We used the highest spectroscopic grade solvents obtained from Sigma-Aldrich. All of the materials were used as received without any further purification.

5.1.1 Preparation of PVA films

The procedure of making PVA films with fluorescence dyes ($ATOTA^+$) was described in a previous study[30]. Briefly, 30 g of PVA powder was slowly added to 170 ml hot doubly distilled water (80-90 ˚C) in a 250 ml flask placed on the temperature controlled hotplate. The mixture was stirred continuously using a magnetic stirring bar for two hours at the same temperature to achieve homogeneous mixing. During the stirring process, air bubbles may form aggressively. The resulting homogeneous solution was allowed to cool down to room temperature overnight to clear out all of the bubbles. Clear PVA solution was obtained without any precipitation. In the next step, 6 ml of PVA solution was poured into a 20 ml glass vial and heated to 40-50 ˚C on a hot plate. To 6 ml of PVA a small volume of 1.44 mM $ATOTA^+$ stock solution (6, 25 and 250 ul respectively to achieve 0.007, 0.03 and 0.30 OD films) was added. The solutions were mixed thoroughly for 10-15 minutes to assure complete mixing. After mixing, the solutions were sonicated for 5-7 minute to eliminate all of the air bubbles. Finally, the solutions were poured into the 2-inch diameter plastic Petri-dishes on a flat balanced surface and stored them in a moisture free, dark environment. PVA films usually take 4 to 6 days to dry.

5.1.2 Preparation of lipid vesicles

Lipid vesicles were prepared from DMPC (1,2-dimyristoyl-sn-glycero-3-phosphocholine). Typically an appropriate amount of lipid and ATOTA dye was dissolved in chloroform in a glass vial to achieve lipid: dye ratio of 800:1. The lipid concentration was 0.2 mM in the glass bottle. The chloroform was evaporated under a constant oxygen-free nitrogen stream and was kept under the chemical hood to remove any remaining organic solvents. Next, PBS (phosphate buffer saline) was added to the solution and sonicated in a bath sonicator at about 40 ˚C for 30 minutes. Poly-disperse vesicles of 100-300 nm size were obtained.

5.1.3 Spectroscopy measurements

5.1.3.1Absorption and linear dichroism

The UV-Vis absorption spectra of $ATOTA^+$ in solvents were measured with a Cary 60 UV-Vis Spectrophotometer (Agilent Technologies). The PVA films doped with $ATOTA^+$ were stretched using a home-built stretching apparatus (Figure 21) that allowed uniform stretching up to 4 times of the original length with heating control; then linear dichroism measurement was performed using Cary 60 UV-Vis Spectrophotometer with an adapted home built PVA films holder and a wire-grid polarizer (Figure 22**)**. Two orthogonal absorption components $A_{\parallel}(\lambda)$ and $A_{\perp}(\lambda)$ for which the light polarized parallel (∥) and perpendicular (⊥) to the stretching direction respectively were measured. Those two components allowed us to calculate the dichroic ratio.

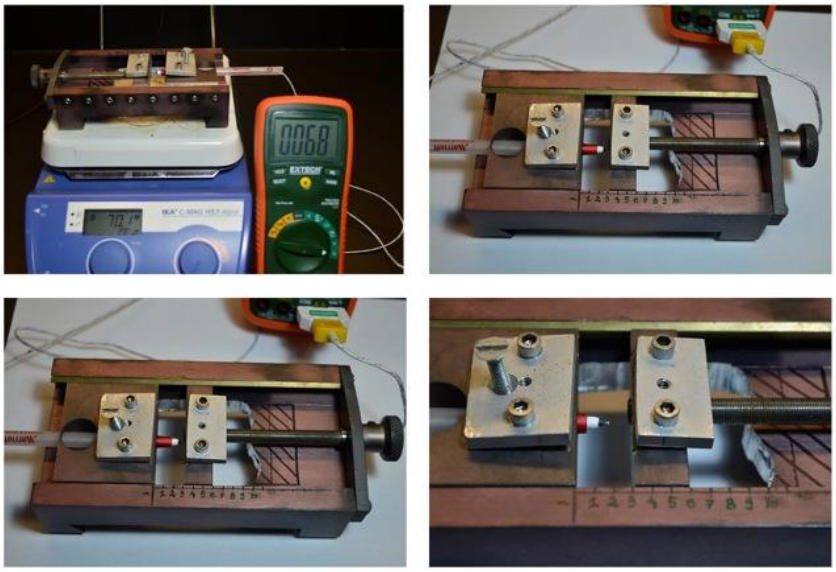

Figure 21: Photographs of the home-built stretching/heating instrument

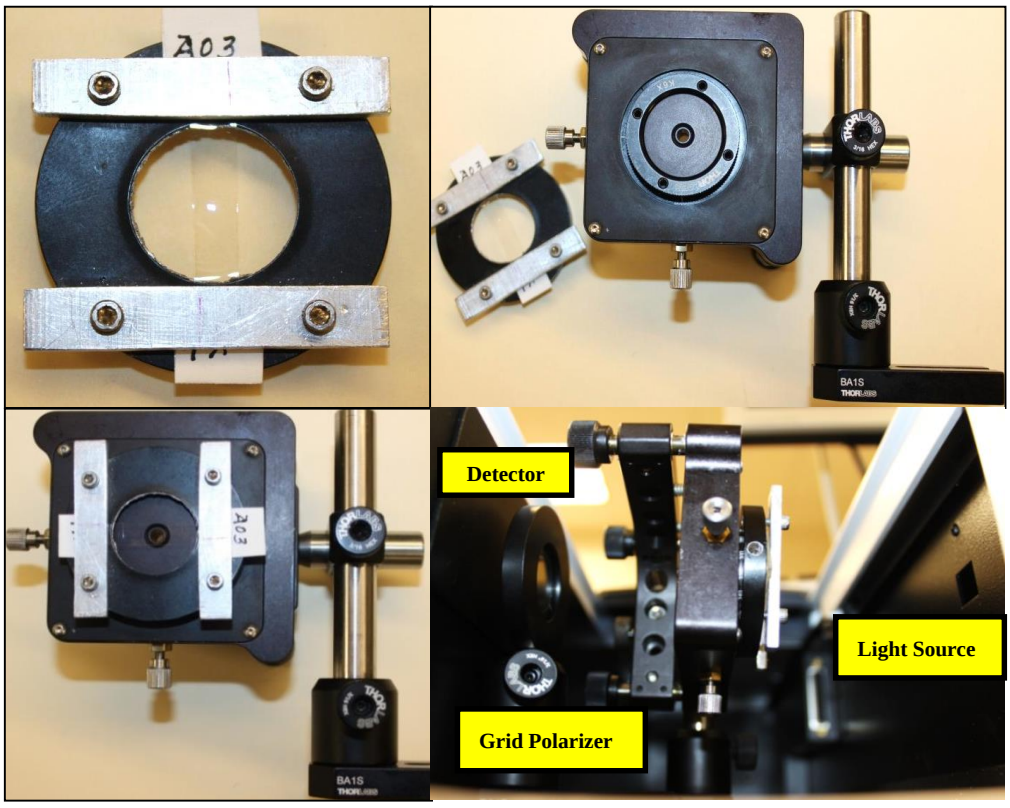

Figure 22: PVA film holder for Linear Dichroism measurement

5.1.3.2 Fluorescence and Fluorescence anisotropy

Fluorescence spectra of $ATOTA^+$ in solvents were measured with a Cary Eclipse Fluorescence Spectrometer (Varian Inc.). The measurements of $ATOTA^+$ samples in solutions were performed in square geometry using 4x10 mm quartz cuvettes, with stoppers at room temperature. To obtain fluorescence spectra in PVA films, an ISS K2 fluorometer (ISS Inc.) was used, which had a custom built front-face adapter fitted to a square geometry setup (Figure 23). Fluorescence anisotropy was also measured with the same instrumentation configuration, including two polarizers placed before and after the sample.

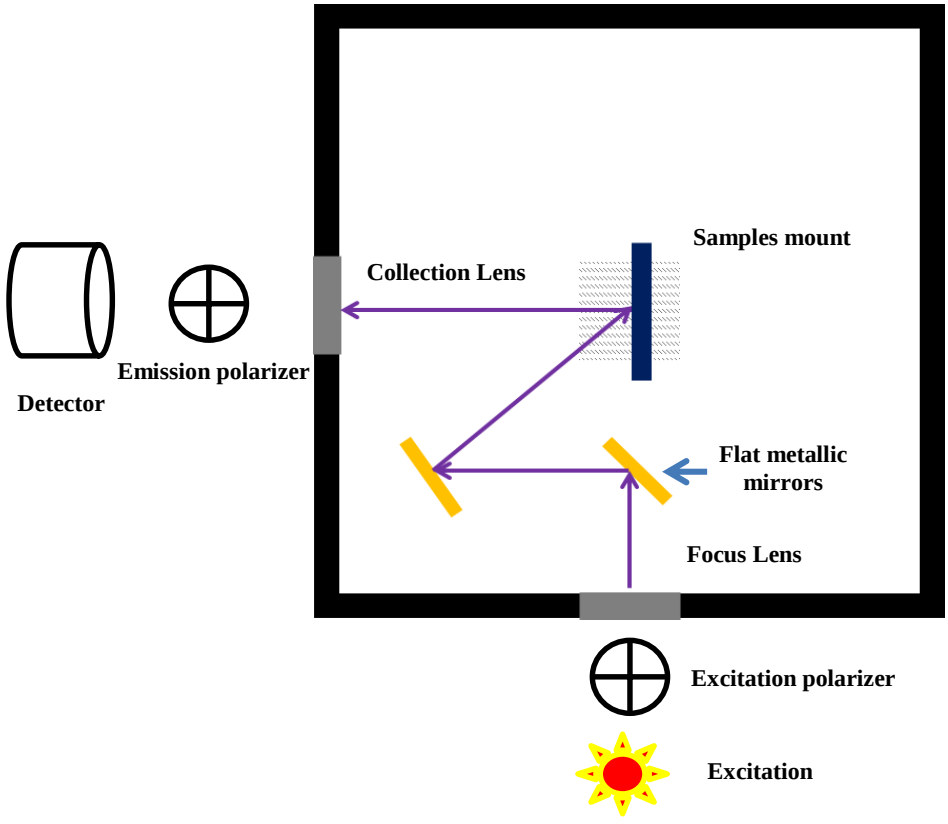

Figure 23: Schematic of front-face setup for $ATOTA^+$ in PVA fluorescence

5.1.3.3 Quantum yield

The quantum yields of $ATOTA^+$ in different organic solvents were determined by integrating the fluorescence intensity of the sample in each solvent and comparing to that obtained from fluorescein in 0.1M NaOH solution as reference. Fluorescein in 0.1M NaOH solution has a known quantum yield of 0.92[31].

5.1.3.4 Fluorescence lifetime and anisotropy decay

Fluorescence lifetime of $ATOTA^+$ was measured using a Fluotime 300 High-Performance Fluorescence Lifetime Spectrofluorometer with Picoharp 300 TCSPC Module (PicoQuant, GmbH). The excitation source for lifetime measurements was the high-power, ultra-broadband white light Laser System Supercontinuum SC450-PP (Fianium, Inc.), which created laser pulses with a pulse width less than 6 ps and 5 MHz repetition rate. The laser excitation wavelength was selected using a prism monochromator. The emission of $ATOTA^+$ was detected by using an R3809U-50 micro-channel plate photomultiplier tube (MCPPMT, Hamamatsu, Inc). The system IRF was measured to be less than 100 ps. The fluorescence lifetime was measured at the magic angle condition (54.7°) to eliminate the depolarization effects. Then the data was analyzed using FluoFit Program (PicoQuant, GmbH, Version 4.4) with a discrete multi-exponential model

$$I(t) = \sum_i \alpha_i e^{-t/\tau_i} \tag{37}$$

where α_i is the amplitude of the i^{th} component's decay at time t and τ_i is the lifetime of the i^{th} element. The intensity weighted average lifetime$< \tau_f >$ and amplitude average lifetime $< \tau_a >$ were calculated using the following equations

$$< \tau_f > = \frac{\sum \alpha_i \tau_i^2}{\sum \alpha_i \tau_i}, < \tau_a > = \frac{\sum \alpha_i \tau_i}{\sum \alpha_i} \quad (38)$$

For amplitude averaged lifetime$< \tau_a >$, α_i is the fractional amplitude.

For anisotropy decays, the intensity decays at vertical and horizontal orientations of emission polarizer were measured, thus allowing us to calculate the time-dependent anisotropy using

$$r(t) = \frac{I_{Parallel}(t) - I_{Perpandicular}(t)}{I_{Parallel}(t) + 2I_{Perpandicular}(t)} \quad (39)$$

The obtained anisotropy decay was analyzed using the Fluofit 4.0 program provided by Picoquant GmbH, Germany, and the collected data was fitted using the formula

$$r(t) = \sum r_i \, e^{-t/\Phi_i} \quad (40)$$

where *r(t)* is the total anisotropy at time *t*, r_i is the fractional anisotropy amplitude associated with the i^{th} component, Φ_i is the rotation correlation time, and *t* is the time in nanoseconds.

5.2 Results and Discussion

5.2.1 Chemical structure

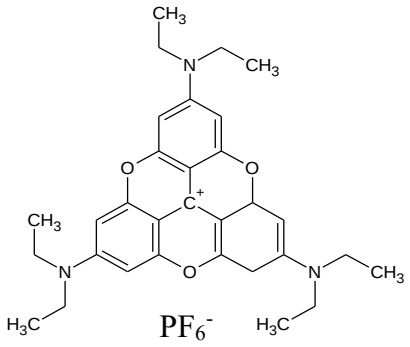

Figure 24: Chemical structure of $ATOTA^+$

Figure 24 shows the chemical structure of $ATOTA^+$. Three dimethylamino groups flank this trioxatriangulenium core structure at the para position to the center carbon cation. The positive carbon charge is delocalized by the electron donating groups surrounding it. Three oxygen bridges help to make the probe molecule rigid.

5.2.2 Absorption

$ATOTA^+$ displays intense absorption in the visible range from 400 nm to 510 nm with absorption peaks around 470–475 nm and almost no absorption in the range of 350 nm to 400 nm or after 525 nm. A shoulder was observed at 440–445 nm. The broadening of the absorption spectra was also observed when going from nonpolar dichloromethane (DCM) to more polar solvents, such as 2-propanol, and dimethylformamide (DMF) as shown in Figure 25.

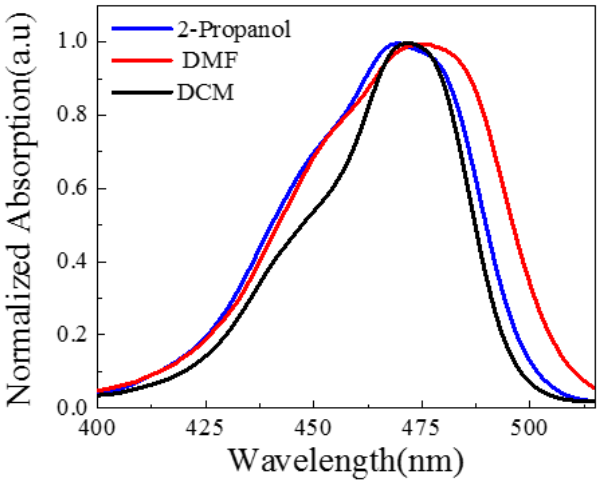

Figure 25: Absorption spectra of $ATOTA^+$ in DCM (black), 2-propanol (blue) and DMF (red)

The absorption width is smallest in DCM, which is the most hydrophobic/nonpolar solvent. The full-width half maxima (FWHM) are 54 nm in DMF, 50 nm in 2-propanol and 41 nm in DCM. The broadening of the absorption must arise from the interactions of $ATOTA^+$ and the solvent molecules. These results further expanded the earlier observations of Laursen and coworkers[3]. The broadening in polar solvents is also possible if more than one underlying transition moment exists, each interact differently with the solvents (see later results and discussion).

5.2.3 Summary of spectral properties of $ATOTA^+$ in organic solvents

Table 1 summarizes the spectral properties of $ATOTA^+$ in some common organic solvents with a wide range of dielectric constants (polarities).

Solvents 460 nm excitation	**Molar Extinction** ($mol^{-1}cm^{-1}$)	Dielectric Constant	**λ_{ab} Max** (nm)	**λ_{Em} Max** (nm)	**QY**	**Life Time** (ns)
DMF	95000	36.7	476	511	0.44	1.66 +/- 0.006
Acetonitrile	98000	37.5	469	506	0.54	2.05 +/- 0.007
Methanol	92000	32.7	470	501	0.6	2.39 +/- 0.008
Tetraethylene Glycol*	97000	15.7	476	510	0.79	2.55 +/- 0.009
2-Propanol	110000	20.3	468	500	0.72	2.66 +/- 0.009
DCM	135000	8.93	473	496	0.98	3.00 +/- 0.01
Decanol	104000	8.10	472	501	0.95	3.16 +/- 0.01
Triacetin	100000	7.01	474	504	0.92	3.25 +/- 0.01

* Bi-exponential intensity decay – 2.89 ns (0.9) and 0.2 (0.1)

Table 1. Spectral properties of $ATOTA^+$ in solvents

$ATOTA^+$ has outstanding extinction coefficients in most solvents, with the lowest in methanol (92,000 $mol^{-1}cm^{-1}$) and the highest in DCM (135,000 $mol^{-1}cm^{-1}$). The errors in extinction coefficient measurements are less than 2%. A moderate solvent dependence was observed in the absorption spectra. The maximum absorption range lies between 468 nm in methanol and 476 nm in DMF. There wasn't any clear relationship between absorption peaks and solvents'

polarity/dielectric constants. The QY of $ATOTA^+$ in the solvents was determined by using fluorescein's QY in 0.1 M NaOH as a reference. The errors in QY measurements were less than 5%. Overall, $ATOTA^+$ shows exceptional QY in many solvents (≥ 0.9 in DCM, decanol and triacetin, ≥ 0.7 in tetraethylene glycol and propanol, ≥ 0.5 in acetonitrile and methanol, and lowest as 0.44 in DMF).

5.2.4 Fluorescence in organic solvents

From Table 1, $ATOTA^+$ clearly shows solvent dependence in its fluorescence properties. For representation purposes, only the excitation and emission of $ATOTA^+$ in three solvents DCM, 2-propanol, and DMF (Figure 26) were shown.

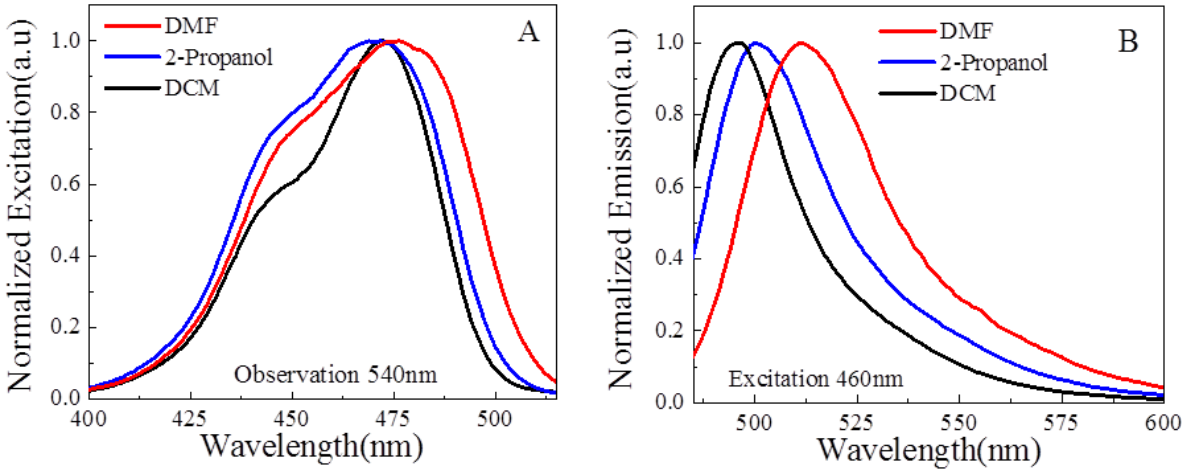

Figure 26: Fluorescence spectra in DCM (black), 2-propanol (blue) and DMF (red) (A) – Excitation (B) – Emission

The excitation spectra resemble the absorption spectra in Figure 25. The emission spectra show a moderate solvent dependence with peaks that vary between 496 nm in DCM, 500 nm in 2-propanol, and 511 nm in DMF.

5.2.5 Fluorescence lifetimes

Results are summarized in Table 1. The fluorescence intensity decays of ATOTA$^+$ can be described with single lifetime component in all pure solvents except tetraethylene glycol with two components (2.89 ns (0.9) and 0.2 ns (0.1)). The fluorescence lifetimes vary between 1.66 ns in DMF to 3.25 ns in triacetin. QY's range is between 0.45 and 0.98. A correlation between the fluorescence lifetime and QY of ATOTA$^+$ (Figure 27A) was observed; as the lifetime increases, so does the QY (the dependence is linearly fitted with a 0.95 regression coefficient R^2). The error bars of the lifetimes are within the points.

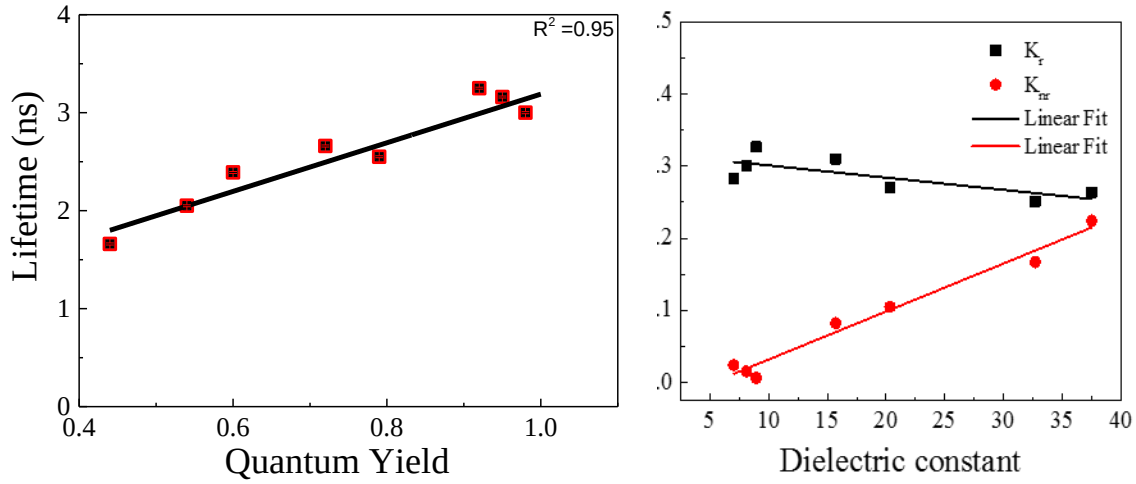

Figure 27: (A) Relationship between QY and lifetime in solvents (B) relationship between radiative and non-radiative rate and dielectric constant with linear fit

Also, as the dielectric constant decreases (thus lowering the polarity), the lifetimes and QY go up linearly. This dependence of ATOTA$^+$'s lifetime and QY on the solvent dielectric constant suggests a reduction in the non-radiative decay rate when the molecule is in non-polar environments owing to the minimal interactions of the dye with the solvent' molecules. Figure 27B confirms the linear relationship between the radiative and non-radiative decay rate with the

dielectric constant. As the dielectric constants increases, while the radiative decay rate changes very slightly in value, a steep increase was observed in the non-radiative decay rate as the interactions with the environment increase.

5.2.6 Fluorescence anisotropy

Figure 28 represents $ATOTA^+$ fluorescence and fluorescence anisotropy in isotropic PVA film. The fluorescence spectra were corrected by subtracting the background signal of the blank PVA isotropic film (without dye). The background noise at emission peaks is below 0.1% of the $ATOTA^+$ signal in the films in all measurements. The fluorescence anisotropies were calculated from the background-subtracted fluorescence spectra.

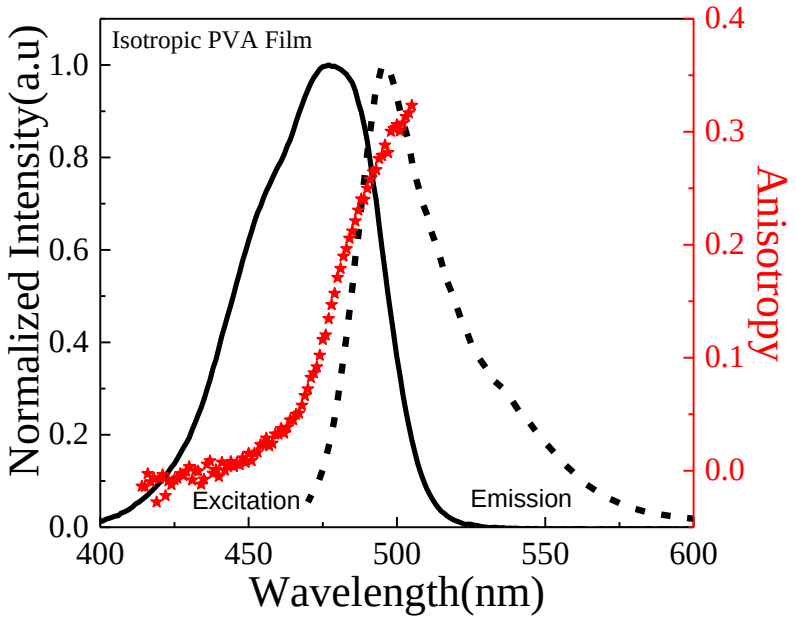

Figure 28: Excitation anisotropy spectra of $ATOTA^+$ in isotropic PVA film

In isotropic PVA films, $ATOTA^+$'s excitation and emission maxima are 475 nm and 497 nm respectively. The excitation spectra and anisotropy were collected by observing the emission at

540 nm. The emission spectrum was observed with excitation wavelength λ_{ex} = 475 nm. The excitation spectrum of $ATOTA^+$ in PVA film has a similar shape as compared to the low polarity solvents, as seen in Figure 26A. In PVA matrices, $ATOTA^+$ exists as a monomer. Excitation anisotropy is close to 0 in 425 nm to 450 nm range, and then it shows a steep increase up to the value of 0.35 above 510 nm and continues to grow. The shape of the calculated excitation anisotropy in relationship to absorption spectrum suggests the presence of more than one underlying transition moment. Also, the rising trend of the excitation anisotropy suggests there is an overlap among the transition moments with significantly different directions. As the contribution of one transition moment with low anisotropy drops with wavelength increase, the system anisotropy increases due to the input from the other high anisotropy transition moment increases and continues to rise beyond 510 nm.

To investigate concentration dependence, two PVA films of different $ATOTA^+$ concentrations were prepared. Figure 29A shows the excitation anisotropy in these two films.

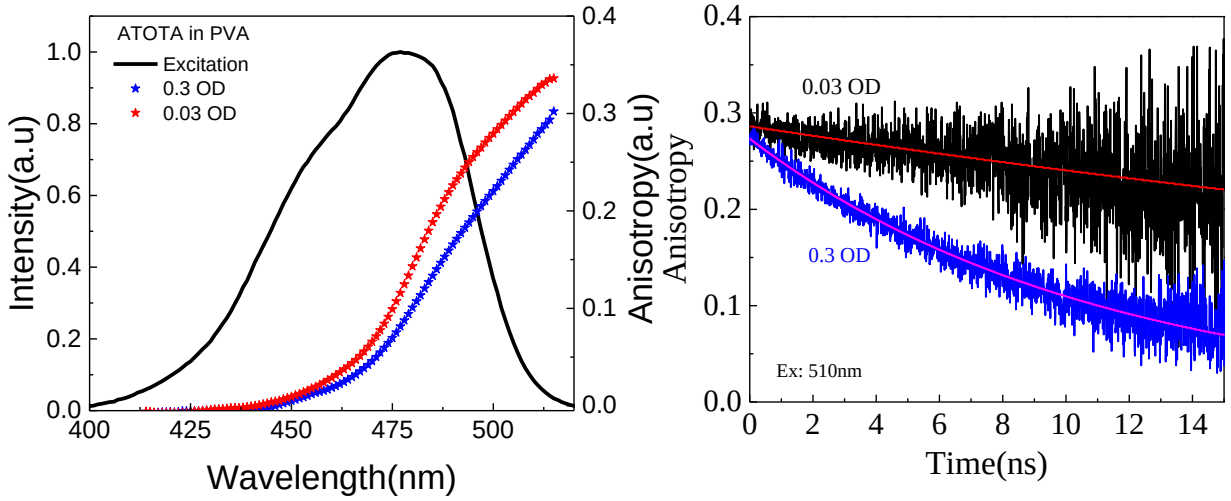

Figure 29: (A) Excitation Anisotropy spectra and (B) Anisotropy Decay in isotropic PVA films

The values of excitation anisotropy decrease with increasing concentrations (OD). In the films with 0.3, and 0.03 OD, the anisotropy at 510 nm is 0.275, and 0.30 respectively. Based on the significant overlap between the $ATOTA^+$ absorption and emission spectrum (Figure 28), a distance between the donor and acceptor fluorophore, also known as the Förster distance, to be between 35 Å and 40 Å is expected for a homo-transfer. With such Förster distance parameter, energy migration at higher concentrations is possible, which will result in decreased limiting anisotropy. Also the anisotropy decays of these two films were also measured. Figure 29B shows the anisotropy decays for PVA films of OD 0.3 and 0.03. Since $ATOTA^+$ molecules were immobilized in the PVA matrix, they must not experience any rotational diffusion and the resulting correlation time should be infinite (or very long). The time-dependent decrease in anisotropy observed suggests the presence of energy transfer. The initial excitation, with vertically polarized light, preferably excites the fluorophores, which are aligned vertically (the process is called photoselection). The vertically oriented molecules will transfer energy to nearby molecules, which have different random orientations. This process continues within the fluorescence lifetime of the probe. As a result, the emitted photon from a molecule will have a different polarization compared to the one initially absorbed. The observed anisotropy reflects this energy migration process. A similar phenomenon was observed by P. Bojarski *et al*[32] in a study of the energy migration of 3,3'-diethylthiacarbocyanine iodide (DTCI) in a similar PVA system. Our results are somewhat surprising. Based on a random distribution of probes in the volume available, energy migration was not expected, even at much higher concentrations. One possible explanation is the affinity between $ATOTA^+$ molecules, resulting in non-random distributions that bring probe molecules much closer together.

5.2.7 Linear dichroism

To understand this anisotropic behavior, the linear dichroism (absorption anisotropy) of the molecules in PVA matrix was studied. Figure 30 shows the polarized absorption, and dichroic ratio as measured in the PVA stretched film.

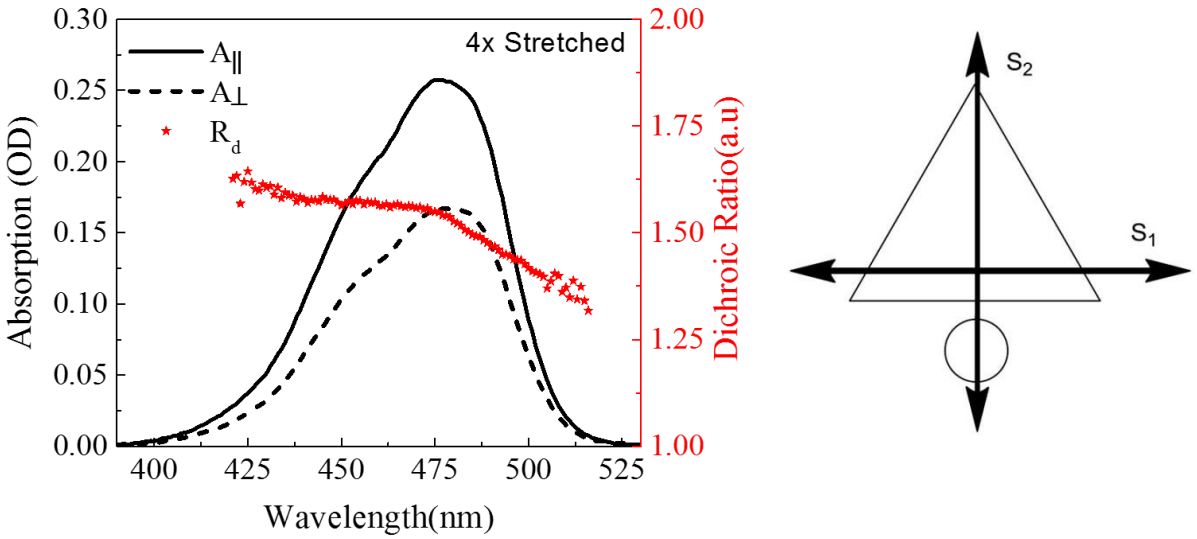

Figure 30: Polarized absorption, linear dichroism and assigned transition moments of ATOTA$^+$ in stretched PVA film

For molecules with a single transition moment (e.g., LDS 798[30]), the dichroic ratio has a constant value that depends on the molecule orientation. For molecules with multiple transition moments, the dichroic ratio is no longer a constant value. For ATOTA$^+$, the dichroic ratio result indicates the presence of the two differently oriented absorption transition moments with the long wavelength absorption band. The dichroic ratio of ~1.5 implies the orientation of ATOTA$^+$ molecule is in nearby region to those planar molecules as in the bottom right of Figure 13. Westerlund *et al*[33] observed the presence of two transitions of ATOTA$^+$ in benzene as well as in DCM upon the binding with a counterion. They further confirmed the presence of two transition moments by

using excitation energy calculations[34]. Our LD results in PVA film provided additional confirmations of the previously published expectation.

5.2.8 Aggregation in aqueous media

$ATOTA^+$ has a potential to be a superior probe as compared to AO in mucus secretion[35]. We conducted studied of aggregate formation of $ATOTA^+$ in aqueous media. $ATOTA^+$ is very hydrophobic (solubility less than 20 nM) due to its core ring and the presence of 6 ethyl groups. Due to this hydrophobic nature, $ATOTA^+$ has a tendency to form aggregates in aqueous environments. Figure 31 illustrates the absorption spectrum of a saturated solution of $ATOTA^+$ in 10% 2-Propanol 5 mM Tris buffer solvent. The presence of 10% 2-Propanol helps increase the solubility and allows us to carry out these measurements.

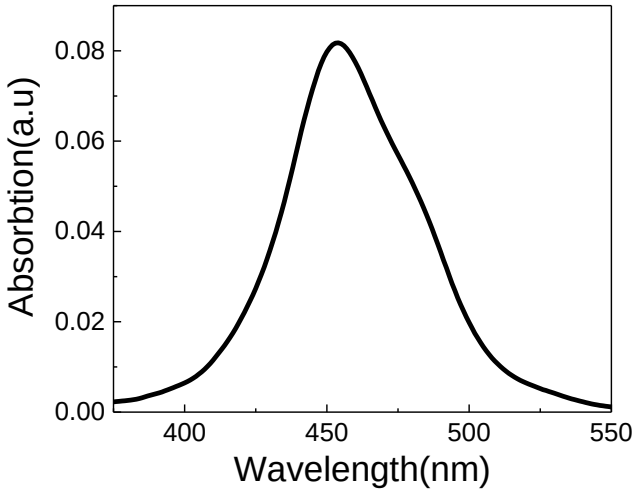

Figure 31: Absorption of 1.25uM $ATOTA^+$ in 10% 2-Propanol 5mM Tris buffer

The absorption spectrum of saturated $ATOTA^+$ in aqueous solution is blue shifted with λ_{ab} maximum at 450 nm. Recall the absorption peaks in several organic solvents are between 468 nm to 476 nm (Table 1). Larson *et al.*[3] previously observed the absorption peak at 450 nm and assigned

to the $ATOTA^+$ ion pair dimer. The emission spectra (results not shown) had two peaks around 510 nm and 580 nm. The 510 nm peak is due to a residual monomer population, and 580 nm represents a dimer/aggregate.

The excitation spectra were measured with observations at 610 nm for a saturated solution (1.25 μM) and 530 nm for diluted (0.125 nM) $ATOTA^+$ solution. The 610 nm observation wavelength is biased towards dimer/aggregate and 530 nm towards monomer (Figure 32A).

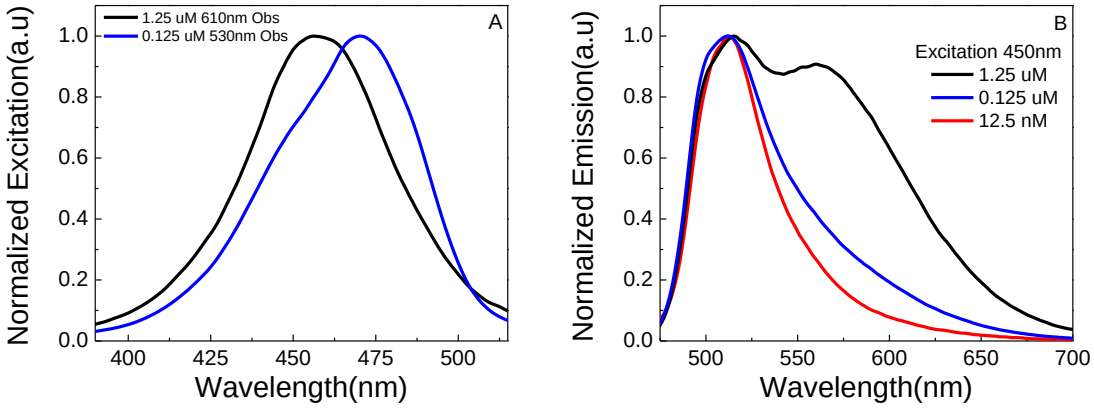

Figure 32: Fluorescence of 1.25uM $ATOTA^+$ in 5mM tris buffer containing 10% 2-Propanol

The 0.125 μM solution shows a maximum at 475 nm and a shoulder at 450 nm in the excitation spectrum corresponding to the absorption peaks of the monomer and dimer/aggregate, respectively. The excitation spectrum of a saturated solution (1.25 μM) on the other hand has the main peak at 450 nm and a shoulder at 475 nm. These changes reflect increased monomer population upon dilution. The result for 12.5 nM solution is similar to that for 0.125 μM sample and is not shown. The concentration dependence of emission was also investigated using a 450 nm excitation wavelength (Figure 32B). The lowest concentration (12.5 nM) shows a peak at 510 nm reflecting the monomer species. Upon increasing the concentration to 0.125 μM, a broadening of the spectrum was observed, with relatively more intensity in the red region. The saturated solution (1.25 μM) has a distinct second peak around 580 nm and significantly higher intensity in red region

indicating the clear presence of the dimer/aggregate population. The absorption spectrum of 1.25 μM ATOTA$^+$ (Figure 31) has the absorption peak at 455 nm, which suggesting most if not all of ATOTA$^+$ is present as dimer/aggregate. Taking these two sets of observations suggests the dimer/aggregate has a significantly lower (>10 fold) QY when compared to that for the monomer. Those behaviors are expected from H-aggregates[36](H stands for a hypsochromic shift in the absorption, a characteristic property of face-to-face stacking aggregation). It should be noted that ATOTA$^+$ is a planar molecule and can form H-aggregate.

5.2.9 Emission spectra at multiple concentrations

In the light of our previous study of AO in mucus secretion[35], the aggregation studies of ATOTA were expanded due to the similarity behavior of ATOTA as compared to AO while forming aggregates. The goal is to evaluate the effect of concentration on the emission spectrum. Figure 33 shows emission spectra of ATOTA$^+$ in 10% 2-Propanol 5 mM Tris buffer solvent at various concentrations.

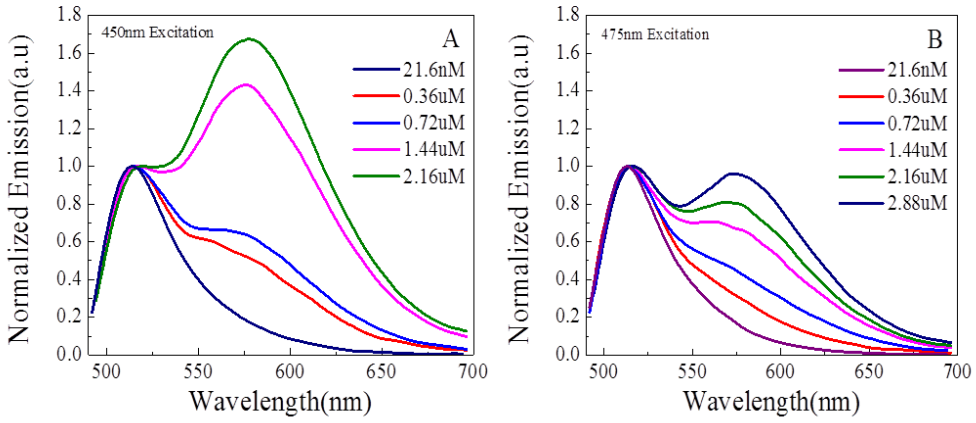

Figure 33: Concentration dependent emission spectra of ATOTA$^+$ (A) 450 nm excitation and (B) 475 nm excitation

The concentrations vary from 21.6 nM to 2.16 μM. The excitation wavelengths are 450 nm (dimer/aggregate peak) and 475 nm (monomer peak). Note that the emission spectra were normalized to the 510 nm peak. The results indicate that the higher the concentration, the higher the λ_{em} peak intensity at 580 nm as compared to at 510 nm. The same trend was observed with both excitations. However, the dimer/aggregate peak (red) is more pronounced when the sample is excited at 450 nm. This is expected as the dimer/aggregate peak is close to 450 nm. This effect is reversible by dilution as the 2.16 μM sample is diluted 100 times (equivalent to 21.6 nM) and re-measured. Now the peak at 580 nm disappears as the aggregates disassociate into monomers, and the narrow emission is associated with the 510 nm peak.

Without any ambiguity, $ATOTA^+$ in 10% 2-Propanol 5 mM Tris buffer solvent was concluded to contains both monomers and aggregates. The distribution of each population depends on the concentration of the dye. The higher the concentration of the dye, the greater the population of the aggregates is in the system. As a result, the emission spectrum of such conditions will be a superposition of the emission spectra of both monomer and aggregate forms. Figure 34 represents the deconvolution of the 2.16 μM sample (excitation 475 nm) spectrum with the monomer emission spectrum (21.6 nM). The monomer has an emission maximum at 510 nm while the recovered dimer/aggregate emission maximum is at 580 nm.

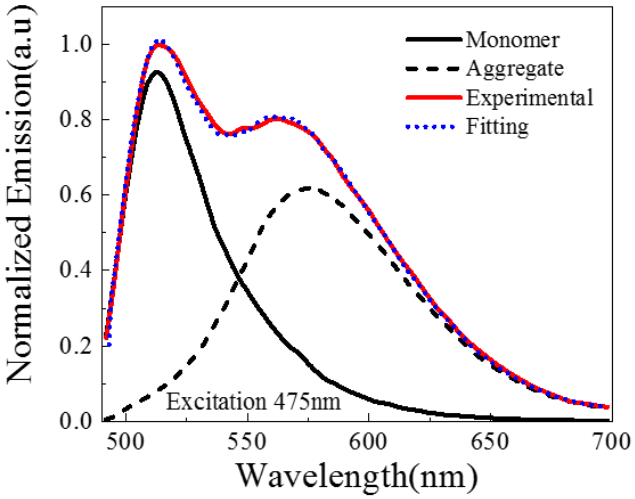

Figure 34: Fitting of emission spectra for monomer and aggregate

5.2.10 Fluorescence lifetimes in buffer solution containing 10% 2-Propanol

The lifetimes of $ATOTA^+$ were then measured in aqueous solution (containing 10% 2-Propanol) at 530 nm and 610 nm. Excitation used was 450 nm. Chi square for the fluorescence lifetime fitting is between 0.9 to 1.1. Results are given in Table 2.

Sample	Lifetime (ns)		Amplitude Fraction		Intensity Fraction		$<\tau_{amp}>$* (ns)	$<\tau_{int}>$** (ns)
	τ_1	τ_2	a_1	a_2	f_1	f_2		
530 nm Observation								
1.25 μM	1.72±0.02	35.5±1.33	0.99	0.01	0.87	0.13	6.02	1.95
125 nM	1.64±0.01	3.03±0.03	0.78	0.22	0.65	0.35	1.95	2.13
610 nm Observation								
1.25 μM	1.76±0.07	37.8±0.22	0.73	0.27	0.11	0.89	33.8	11.5

* Amplitude Weighted Average Lifetime
** Intensity Weighted Average Lifetime

Table 2: Lifetimes of $ATOTA^+$ in mixed aqueous solvents

Notice that the earlier emission spectra in 10% 2-Propanol indicated two distinct emission peaks at 510 nm and 580 nm, which corresponded to the emissions of monomer and dimer/aggregate

species respectively (Figure 34). Therefore, the lifetimes of $ATOTA^+$ at 530 nm and 610 nm (experimental setting) were investigated to selectively measure the lifetimes of the monomer and dimer/aggregate forms (Figure 35). The intensity decays at 530 nm indicate the presence of two lifetimes. In the case of saturated concentration (1.25 μM), the 1.752 ns component is dominant as it contributes about 88% of fluorescence intensity. Based on the deconvoluted spectra, the long-lived dimer/aggregate (35.5 ns) is expected to only make a small contribution at 530 nm. Similarly, monomer species will also be a minor presence at 610nm. The dilution to 0.125 μM concentration shifts the equilibrium towards the monomer population, which corresponding to the major fluorescence at 530 nm from the monomer species (0.985 fractional intensity). These results conclude that the red emitting long-lived species is almost absent from the blue edge of the emission spectra and our previous fit of the monomer/dimer emission spectra in Figure 34 is reasonable. Furthermore, the monomer lifetime of around 1.75 ns to 1.8 ns suggests that in aqueous media, the quantum yield of $ATOTA^+$ will be closer to that in DMF and acetonitrile (0.44 to 0.54) rather than in the nonpolar DCM.

For 1.25 μM sample at 610 nm observation (dimer/aggregate emission), two lifetimes were again observed. The shorter lifetimes of 1.76 ns (monomer) now only contributes about 12% of the fluorescence while the dimer/aggregate (37 ns) dominates the fluorescence. These results are overall in line with the steady state spectrum (Figure 35). The longer lifetime of the dimers/aggregates as compared to the monomer species is expected from H-aggregate[36]. Laursen *et al.*[3] also observed long fluorescence lifetimes in the case of dimer/aggregate in heptane.

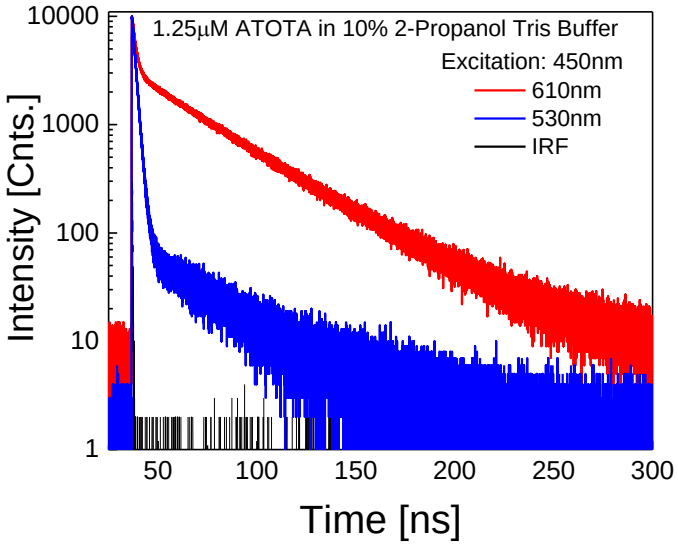

Figure 35: Intensity decays of ATOTA$^+$ in 10% 2-Propanol Tris buffer

5.2.11 ATOTA$^+$ in lipid bilayer

5.2.11.1 Fluorescence in DMPC

The spectral properties of ATOTA$^+$ in lipid vesicles were also characterized. DMPC (1,2-dimyristoyl-sn-glycero-3-phosphocholine) is one of many lipids within the phosphatidylcholine lipid family that is highly abundant in biological membranes and has therefore drawn much attention for biophysical studies. Figure 36 illustrates the excitation spectra of ATOTA$^+$ at 550 nm observation and the emission spectra at 440 nm excitation in DMPC at room temperature.

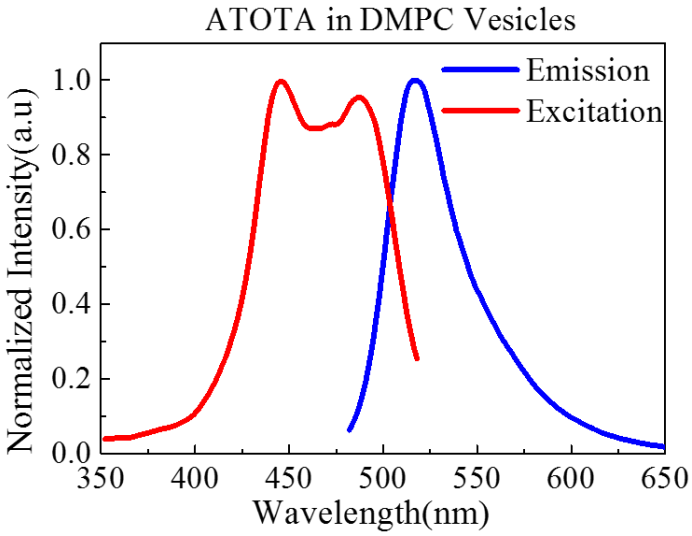

Figure 36: Excitation (red line) and emission (blue line) spectra of $ATOTA^+$ in DMPC at room temperature

In DMPC, the excitation spectra show two clear peaks at 446 nm and 487 nm, suggesting the formation of the ion pair. The emission spectra have emission maxima at 518 nm, which is relatively shifted toward the red compared to the emission peak in polar solvents in Table 1. This excitation spectrum is similar to the absorption spectra (result not shown). The excitation spectrum profile is different from previous observation in several organic solvents (Table 1). Laursen *et al.*[34ESI] earlier saw a similar splitting of excitation spectrum into two peaks in DCM and benzene[34] upon addition of the counterion PF_6, and assigned this splitting to the separation of two underlying transition moments. The shape of the excitation spectra, which usually represents the case when $ATOTA^+$ and counterion are dissolved in hydrophobic nonpolar solvents; therefore, suggesting that $ATOTA^+$ is more likely presenting in the inner leaflets of the bilayer (hydrophobic environment). Being a charged molecule, $ATOTA^+$ needs the counterion PF_6^- to become neutral. We did not look at the localization of the probe in the bilayer. However, based on the spectral

splitting, it is likely for ATOTA$^+$ to be excluded from water molecules and be present in the hydrocarbon interior. Laursen *et al.*[37] have also observed the spectral splitting in a bilayer using a hydrophobic fatty acid analog of ATOTA$^+$.

5.2.11.2 ATOTA$^+$ in dioxane

Figure 37 represents the absorption and non-corrected excitation spectra of ATOTA$^+$ in dioxane, which is a nonpolar solvent. The splitting in the absorption spectrum suggests the ion pair formation of ATOTA$^+$ as seen previously in benzene and other nonpolar solvents[3]. The excitation spectrum well resembles the absorption spectrum, indicating the presence of only one species.

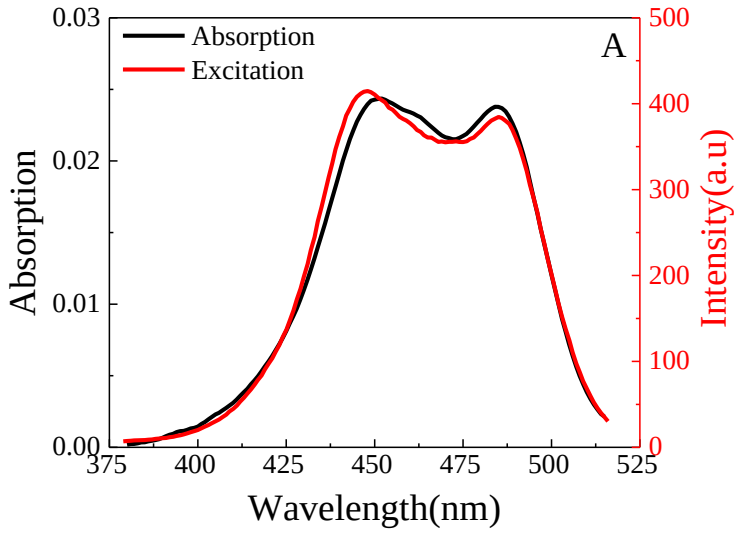

Figure 37: Absorption and excitation spectra of ATOTA$^+$ in dioxane (non-corrected)

5.2.11.3 Fluorescence lifetime in DMPC

In Table 3, the lifetimes of ATOTA$^+$ in DMPC at three different temperatures (at, below and above the phase transition temperature for DMPC) were presented.

T(^{0}C)	Lifetimes (ns)			Amplitude Fractions			$<\tau_{int}>$ (ns)	$<\tau_{amp}>$ (ns)	χ^2
	τ_1	τ_2	τ_3	a_1	a_2	a_3			
15	2.73±0.02	4.19±0.06	24.7±1.47	0.788	0.209	0.003	3.64	3.10	0.99
23	2.55±0.02	4.36±0.11	33.0±3.14	0.915	0.083	0.002	3.39	2.75	1.02
30	2.08±0.01	4.32±0.17	15.2±3.55	0.972	0.027	0.001	2.28	2.15	1.10

Table 3: Lifetimes of ATOTA$^+$ fluorescence in DMPC at different temperatures

The sample was excited at 440 nm and observed the fluorescence at 518 nm. The intensity decays can be described by three lifetime components. The two short components of a few nanosecond timescales those are responsible for over 99% of the population. As the longer lifetime component of approximately 20 ns makes up less than 1%, we can conclude the absence of dimers/aggregate at these minuscule probe fraction ratios (800:1 lipid: dye ratio). As the temperature decreases from room temperature to 15 °C, an increase in the lifetime values was found. Similarly, with the increased temperature, the values of the lifetime decrease at 30°C. A shift in the population towards the shorter lifetime component was further observed. Overall, the increase in temperature results in a reduction in both the amplitude and intensity averaged lifetime, which is expected due to the increased non-radiative rate with increasing temperatures. The presence of two shorter lifetime components indicates the heterogeneity of ATOTA$^+$'s environment.

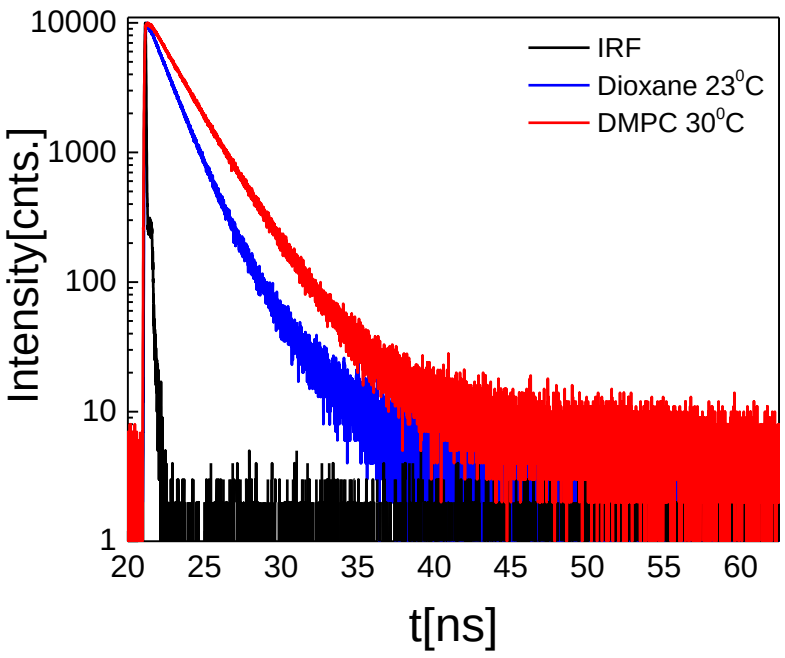

Figure 38: Intensity decay of ATOTA$^+$ in DMPC at 23° C

Figure 38 shows the intensity decay of ATOTA$^+$ in dioxane compared to DMPC. A faster decay rate with multiple components was observed. The fluorescence lifetime in dioxane included three components 0.2 ns (0.1), 1.4 ns (0.87) and 3.5 ns (0.03); the 1.4 ns population is the main species. The amplitude-weighted lifetime is 1.36 ns as compared to 3 ns in DCM. The results in dioxane are similar to those found in the lipid bilayer, which further suggests the probe is present in the hydrocarbon core rather than the interfacial region of the bilayer.

5.2.11.4 Tentative localization of ATOTA$^+$ in Bilayer

Being a hydrophobic molecule, ATOTA can be possibly utilized as a membrane probe. Primarily based on lifetime results, we propose a tentative localization of ATOTA$^+$ in the bilayer. The cartoon (Figure 39) is only a crude approximation suggesting its presence in the upper region of

the hydrocarbon core and exclusion from the aqueous phase. It will take more extensive experimentation to make a more precise localization.

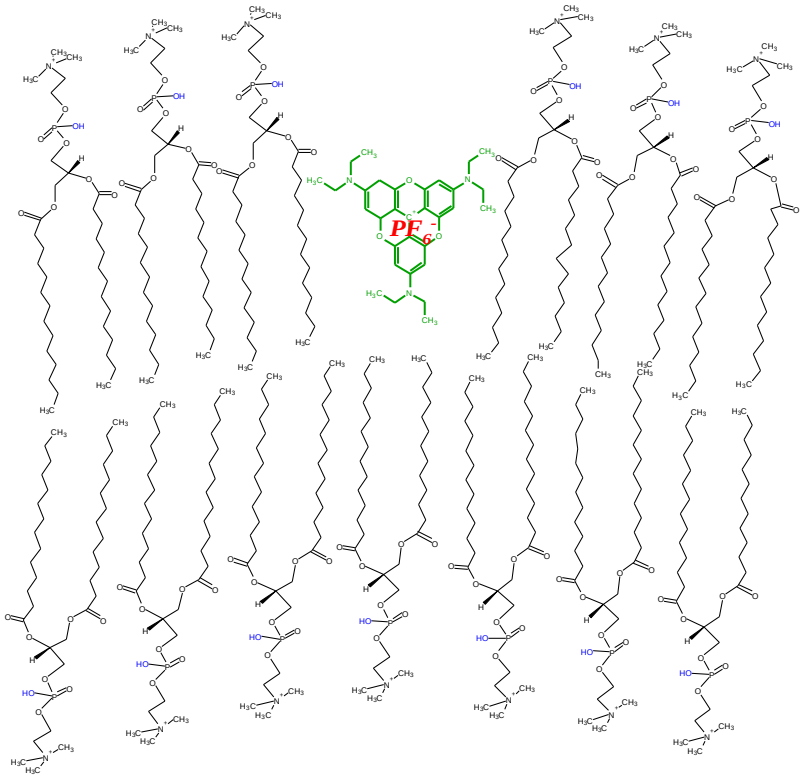

Figure 39: Cartoon illustrates the localization of ATOTA$^+$ in bilayer

5.3 Summary/Conclusions

Our results strongly indicated that ATOTA$^+$ is a very promising green fluorophore. With a size comparable to or smaller than most green fluorophores, ATOTA$^+$ is very attractive as its molar extinction is the highest among commonly used green fluorophores such as fluorescein and BODIPY. An advantage of ATOTA$^+$ is that its excitation maxima match with the widely used diode laser light source of 475 nm, while comparable fluorophores such as fluorescein and fluorescein-like molecules with their excitation maxima at about 495 nm give up between 40%

and 60% of the absorption at 475 nm excitation. $ATOTA^+$'s molar extinctions in the range of 95,000 $mol^{-1}cm^{-1}$ in polar DMF to 135,000 $mol^{-1}cm^{-1}$ in nonpolar dichloromethane were observed. The absorption and emission of $ATOTA^+$ are only moderately sensitive to the hydrophilicity/polarity of the solvents. The main effect of solvent polarity is to make the absorption of $ATOTA^+$ somewhat broader, resulting in a decrease in the peak extinction coefficient. The absorption maximum is less than 8 nm different and does not follow the solvent polarity trend. The emissions are also modestly sensitive to solvent polarity with an emission maximum of 496 nm in non-polar DCM to 511 nm in very polar DMF. This shift in the emission of $ATOTA^+$ can be compared to polarity-sensitive probes such as PRODAN[38] and DAPOXYL[39], the emission peaks of which shift over 200 nm when going from polar to nonpolar solvent. The emission profile of $ATOTA^+$ is narrower than that of fluorescein, which is in fact, beneficial as it allows collection of most emission photons in a narrow range of wavelength while efficiently separating them from other fluorophores' emitted photons. $ATOTA^+$ has a small Stokes' shift, similar to fluorescein, BODIPY, and other green emitting probes, therefore making it similarly vulnerable to energy migration due to homo-transfer as seen in our anisotropies studies in PVA films (Figure 29).

$ATOTA^+$ has a triangular shape with symmetrical ethyl substitutions at three amines at the para-position to the center carbocation. It is expected to show a degenerate transition moment and a limiting anisotropy of 0.10 across the main absorption transition[6]. Surprisingly the results do not meet this expectation. The excitation anisotropy shows an increase from a value of close to 0 at the blue edge to 0.15 at the absorption peak and continuing to increase to 0.35 approaching the red edge (Figure 29). These results indicate the presence of two overlapping transitions, with the lowest energy one (higher wavelength) oriented close to coplanar with the molecule. The splitting of the main absorption transition into two was, in fact, observed by Laursen *et al.* in

dichloromethane upon addition of the counterion.[34] Further, this group theoretically confirmed and calculated the two transitions to be at close to 90° to each other[34]. We experimentally confirmed the presence of the two transitions by linear dichroism measurements in stretched PVA films (Figure 30).

The planarity of $ATOTA^+$ is favorable to form a face-to-face aggregate, also known as H-aggregate. In fact, Laursen *et al.* observed such aggregation using a fatty derivative analog of $ATOTA^+$ in a planar lipid layer as well as in dichloromethane in the presence of the counterion[37]. In general, the H-aggregate is blue-shifted in absorption and shows a red-shifted emission. As $ATOTA^+$ is a hydrophobic molecule, H-aggregates were observed in an aqueous environment (Figure 31, Figure 32, and Table 2). The absorption maximum of $ATOTA^{+'}$ aggregates is blue shifted by 20 nm while the emission is red-shifted by 60 nm-65 nm. Furthermore, $ATOTA^{+'}$ red-shifted emission is long lived with a lifetime of more than 20 ns. These results suggest a possible application of ATOTA+ as a better substitute for AO (much higher extinction coefficient and QY) in mucin granules secretion study. Furthermore, the hydrophobicity of $ATOTA^+$ allowed us to incorporate it in the DMPC vesicle. The excitation spectra show the splitting of absorption, which is not surprising (Figure 36). The only way a cationic $ATOTA^+$ molecule, even though it is hydrophobic, can enter a lipid hydrocarbon region is by having its charge neutralized by a counterion. The spectral behavior is reproduced in dioxane (Figure 37), further confirming that $ATOTA^+$ is likely to be in the lipid hydrocarbon region rather than the polar head group region. $ATOTA^+$,therefore, can also be used as a membrane probe.

Ultimately, fluorescence output for a probe is a chief concern in these studies. The main attributes involved in determining fluorescence output are absorption extinction coefficient, quantum yield, and fluorescence lifetime. Taken together the molar extinctions of 90,000 $mol^{-1}cm^{-1}$ to 135,000

$mol^{-1}cm^{-1}$, a matching of absorption maxima with one of the most common laser diode light source of 475 nm, a high quantum yield, suggests $ATOTA^+$ be very promising for use as a green fluorophore. As there are three potential substitution sites, making the chemistry relatively easy, it should be possible to create probes of varying charges and /or polarities depending on the needs at hand.

5.4 Future Directions

Despite being cationic, $ATOTA^+$ is hydrophobic due to the presence of 6 ethyl substitutions on its structure. As a result, $ATOTA^+$'s solubility in water is very low (less than 20 nM). Such low solubility promotes the formation of the aggregates of $ATOTA^+$ in aqueous environments. The aggregate formation is highly concentration-dependent. The aggregate form of $ATOTA^+$ is long-lived and red-shifted, compared to its monomer, which allows easy monitoring of the monomer–aggregate equilibrium. In light of our previous study of acridine orange[4], one important potential application of $ATOTA^+$'s aggregation is in biophysical studies of mucus secretion, which are key processes in many respiratory diseases.

In additional, taking advantage of the outstanding extinction coefficient and high QY of $ATOTA^+$, Laursen *at al.* had synthesized a fatty-acid derivative analog of $ATOTA^+$ (Figure 39) by replacing the ethyl groups with long alkyl (n-decyl) chains at one of the amino groups.[28] This fatty acid analog forms ion pair dimer/aggregate in both nonpolar solvents and lipid bilayer films, which make it another potential membrane probe. The ion-pair dimer/aggregate is blue-shifted in absorption and red-shifted in emission. The red-shifted emission is long-lived (30 ns-40 ns) as expected for an H-aggregate. We plan to characterize this $ATOTA^+$ fatty acid derivative systematically as a function of both lipid composition and physical state. The aspects include the localization, internal motions, and monomer- aggregate equilibrium. We hope this new probe will

be an extremely sensitive membrane probe. The long-lived aggregate emission also opens the possibility of time gating of cellular background fluorescence for FLIM and greatly help in FLIM-based studies of cell membrane dynamics.

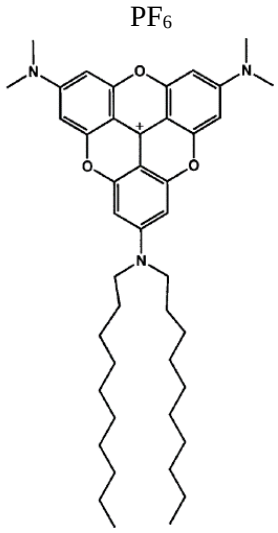

Figure 39: Fatty derivative of $ATOTA^{+}$

Bibliography

1. Dimitry S. *New application of acridine orange to study biophysics of exocytosis processes in cell.* Texas Christian University; 2013.

2. Laursen BW, Krebs FC, Nielsen MF, Bechgaard K, Christensen JB, Harrit N. 2, 6, 10-tris (dialkylamino) trioxatriangulenium ions. synthesis, structure, and properties of exceptionally stable carbenium ions. *J Am Chem Soc*. 1998;120(47):12255-12263.

3. Laursen BW, Reynisson J, Mikkelsen KV, Bechgaard K, Harrit N. 2, 6, 10-tris (dialkylamino) trioxatriangulenium salts: A new promising fluorophore. ion-pair formation and aggregation in non-polar solvents. *Photochemical & Photobiological Sciences*. 2005;4(8):568-576.

4. Shumilov D, Popov A, Fudala R, et al. Real-time imaging of exocytotic mucin release and swelling in calu-3 cells using acridine orange. *Methods*. 2014;66(2):312-324.

5. Jameson DM, ed. *Introduction to fluorescence.* Taylor & Francis; 2014.

6. Joseph RL, Lakowicz R. Principles of fluorescence spectroscopy. 1999.

7. Lakowicz J. Fluorescence spectroscopy of biomolecules, in encyclopaedia of molecular biology and molecular medicine. 1995.

8. Kasha M. Characterization of electronic transitions in complex molecules. *Discuss Faraday Soc*. 1950;9:14-19.

9. Andersen LH, Nielsen IB, Kristensen MB, et al. Absorption of Schiff-base retinal chromophores in vacuo. *J Am Chem Soc*. 2005;127(35):12347-12350.

10. Rocha-Rinza T, Christiansen O, Rajput J, et al. Gas phase absorption studies of photoactive yellow protein chromophore derivatives. *The Journal of Physical Chemistry A*. 2009;113(34):9442-9449.

11. Lewis GN, Calvin M. The color of organic substances. *Chem Rev*. 1939;25(2):273-328.

12. Rurack K, Resch-Genger U. Rigidization, preorientation and electronic decoupling—the 'magic triangle'for the design of highly efficient fluorescent sensors and switches. *Chem Soc Rev*. 2002;31(2):116-127.

13. Treibs A, Jacob K. Cyclotrimethine dyes derived from squaric acid. *Angewandte Chemie International Edition in English*. 1965;4(8):694-694.

14. Becker W. *The bh TCSPC handbook.* Becker & Hickl; 2014.

15. Grinvald A, Steinberg IZ. On the analysis of fluorescence decay kinetics by the method of least-squares. *Anal Biochem*. 1974;59(2):583-598.

16. Badea MG, Brand L. [17] time-resolved fluorescence measurements. *Meth Enzymol*. 1979;61:378-425.

17. Ware WR, Doemeny LJ, Nemzek TL. Deconvolution of fluorescence and phosphorescence decay curves. least-squares method. *J Phys Chem*. 1973;77(17):2038-2048.

18. ThermoFisher. **Fluorescent probes**. https://www.thermofisher.com/us/en/home/life-science/protein-biology/protein-biology-learning-center/protein-biology-resource-library/pierce-protein-methods/fluorescent-probes.html.

19. Bader AN, Hoetzl S, Hofman EG, et al. Homo-FRET imaging as a tool to quantify protein and lipid clustering. *ChemPhysChem*. 2011;12(3):475-483.

20. Tanizaki Y. Dichroism of dyes in the stretched PVA sheet. II. the relation between the optical density ratio and the stretch ratio, and an attempt to analyze relative directions of absorption bands. *Bull Chem Soc Jpn*. 1959;32(1):75-80.

21. Tanizaki Y. The correction of the relation of the optical density ratio to the stretch ratio on the dichroic spectra. *Bull Chem Soc Jpn*. 1965;38(10):1798-1799.

22. Kawski A, Gryczyński Z. On the determination of transition-moment directions from emission anisotropy measurements. *Zeitschrift für Naturforschung A*. 1986;41(10):1195-1199.

23. Thulstrup EW, Michl J, Eggers J. Polarization spectra in stretched polymer sheets. II. separation of. pi.-. pi.* absorption of symmetrical molecules into components. *J Phys Chem*. 1970;74(22):3868-3878.

24. Thulstrup E. *Aspects of the linear and magnetic circular dichroism of planar organic molecules*. Vol 14. Springer Science & Business Media; 2012.

25. Martin J, Smith RG. Factors influencing the basicities of triarylcarbinols. the synthesis of sesquixanthydrol. *J Am Chem Soc*. 1964;86(11):2252-2256.

26. Barker C, Bridge M, Stamp A. 796. steric effects in di-and tri-arylmethanes. part I. electronic absorption spectra of o-methyl derivatives of michler's hydrol blue and crystal violet; conformational isomers of crystal violet. *Journal of the Chemical Society (Resumed)*. 1959:3957-3963.

27. Griffiths J. Colour and constitution of organic molecules. . 1976.

28. Westerlund F, Lemke HT, Hassenkam T, Simonsen JB, Laursen BW. Self-assembly and near perfect macroscopic alignment of fluorescent triangulenium salt in spin-cast thin films on PTFE. *Langmuir*. 2013;29(22):6728-6736.

29. Shi D, Sfintes G, Laursen BW, Simonsen JB. Fluorescent and highly stable unimodal DMPC based unilamellar vesicles formed by spontaneous curvature. *Langmuir*. 2012;28(23):8608-8615.

30. Luchowski R, Sarkar P, Bharill S, et al. Fluorescence polarization standard for near infrared spectroscopy and microscopy. *Appl Opt*. 2008;47(33):6257-6265.

31. Arbeloa FL, Ojeda PR, Arbeloa IL. On the aggregation of rhodamine B in ethanol. *Chemical physics letters*. 1988;148(2):253-258.

32. Bojarski P, Gryczyński I, Kułak L, Synak A, Barnett A. Excitation energy migration between elongated fluorophores in uniaxially oriented polyvinyl alcohol films. *Chemical physics letters*. 2006;431(1):94-99.

33. Westerlund F, Elm J, Lykkebo J, et al. Direct probing of ion pair formation using a symmetric triangulenium dye. *Photochemical & Photobiological Sciences*. 2011;10(12):1963-1973.

34. Westerlund F, Elm J, Lykkebo J, et al. Direct probing of ion pair formation using a symmetric triangulenium dye. *Photochemical & Photobiological Sciences*. 2011;10(12):1963-1973.

35. Shumilov D, Popov A, Fudala R, et al. Real-time imaging of exocytotic mucin release and swelling in calu-3 cells using acridine orange. *Methods*. 2014;66(2):312-324.

36. Maiti NC, Ravikanth M, Mazumdar S, Periasamy N. Fluorescence dynamics of noncovalently linked porphyrin dimers, and aggregates. *J Phys Chem*. 1995;99(47):17192-17197.

37. Shi D, Sfintes G, Laursen BW, Simonsen JB. Fluorescent and highly stable unimodal DMPC based unilamellar vesicles formed by spontaneous curvature. *Langmuir*. 2012;28(23):8608-8615.

38. Parasassi T, Krasnowska EK, Bagatolli L, Gratton E. Laurdan and prodan as polarity-sensitive fluorescent membrane probes. *J Fluoresc*. 1998;8(4):365-373.

39. Diwu Z, Zhang C, Klaubert DH, Haugland RP. Fluorescent molecular probes VI: The spectral properties and potential biological applications of water-soluble dapoxyl™ sulfonic acid. *J Photochem Photobiol A*. 2000;131(1):95-100.

Hung The Doan

6832 Beverly Glen Dr. Fort Worth, Texas 76132. USA
hung.doan@tcu.edu +1(682)521-0280/ +1(469)702-0990

Personal Background

Hung The Doan

Hue, Vietnam

Son of Hieu Doan and Phuong Huyen

Education

- Doctor of Philosophy (Ph.D.) in Biophysics — 2018
  Texas Christian University
  Fort Worth, Texas, USA
- Bachelor of Science in Physics — 2013
  Minor: Mathematics & Chemistry
  John V. Roach Honors College
  Texas Christian University
  Fort Worth, Texas, USA
- Diploma — 2006
  Quoc Hoc High School
  Hue, Vietnam

Experiences

- Research Assistantship, Texas Christian University — 2013-2017
  Development of Fluorescence Technology
  Advisor: Dr. Zygmunt Gryczynski
  Fort Worth, TX, USA
- Teaching Assistantship, Texas Christian University — 2013-2017
  General Physics 1 & 2 Lab (Physics & Non-Physics Major)
  Fort Worth, TX, USA
- Student Research Volunteer, UNT Health Science Center — 2011-2017
  Center for Fluorescence Technologies and Nanomedicine
  Advisor: Dr. Zygmunt Gryczynski
  Fort Worth, TX, USA
- Undergraduate Research, Texas Christian University — 2011-2013
  Development of Fluorescence Technology
  Advisor: Dr. Zygmunt Gryczynski
  Fort Worth, TX, USA

Awards

- University 3 Minute Thesis Competition Champion — 2016
  Judge's 1st Place, People's Choice 1st Place
  Texas Christian University, Fort Worth, Texas USA

	• CSE 3 Minute Thesis Competition Champion Judge's 1st Place, People's Choice 1st Place Texas Christian University, Fort Worth, Texas USA	2015
	• 1st Place Graduate Research –Physics and Astronomy The Michael and Sally McCracken Annual Student Research Symposium. *Multi-pulse pumping for far-field super-resolution imaging* Texas Christian University, Fort Worth, Texas USA	2016
	• 1st Place Undergraduate Research – Physics and Astronomy The Michael and Sally McCracken Annual Student Research Symposium. *Characterization of BODIPY Variants to Determine Optimal Hybridization Potential with an Azadioxatriangulenium (ADOTA) fluorophore(2016)* *Application Of Fluorescent Nanodiamonds For Molecular Binding Detection.(2012)* Texas Christian University, Fort Worth, Texas USA	2016 2012
	• SERC Undergraduate Research Grant $1500 Texas Christian University, Fort Worth, Texas USA	2012- 2013
	• Dr. C.A. Quarles Physics and Astronomy Scholarship $1500 Texas Christian University, Fort Worth, Texas USA	2012
	• The Joseph Morgan Physics Scholarship $1500 Texas Christian University, Fort Worth, Texas USA	2012
	• 2nd Place Jim Bolen Math Competition - Tarrant County Tarrant Community College, Fort Worth, Texas USA	2010
	• 1st Place Jim Bolen Math Competition Tarrant Community College, North West Campus Fort Worth, Texas USA	2010
	• 1st Place Jim Bolen Math Competition Tarrant Community College, North West Campus Fort Worth, Texas USA	2009
Positions & Memberships	• Library Committee Texas Christian University, Fort Worth, Texas USA	2016-2017
	• Graduate Student Representative Physics & Astronomy Department	2016-2017

Texas Christian University, Fort Worth, Texas USA

- Phi Theta Kappa Honor Society 2009
- Society of Physics Students 2010
  Texas Christian University, Fort Worth, Texas USA
- SPIE 2014-2016
- American Physical Society 2015-2017
- Society of Porphyrin & Phthalocyanines 2016-2018

Publications

1. Multiple-pulse pumping for enhanced fluorescence detection and molecular imaging in tissue 2013
   *Rich RM, Gryczynski I, Fudala R, Borejdo J, Stankowska DL, Krishnamoorthy RR, Raut S, Maliwal BP, Shumilov D, **Doan H**, Gryczynski Z. Methods, 66(2), pp.292-298.*
2. Generating multiple-pulse bursts for enhanced fluorescence detection 2014
   *Shumilov D, Rich RM, Gryczynski I, Raut S, Gryczynski K, Kimball J, **Doan H**, Sørensen TJ, Laursen BW, Borejdo J, Gryczynski Z. Methods and Applications in Fluorescence 2, no. 2 (2014): 024009.*
3. Homodimeric BODIPY Rotor as a Fluorescent Viscosity Sensor for Membrane-Mimicking and Cellular Environments 2014
   *Raut S, Kimball J, Fudala R, **Doan H**, Maliwal B, Sabnis N, Lacko A, Gryczynski I, Dzyuba SV, Gryczynski Z. Physical Chemistry Chemical Physics. 2014;16(48):27037-42.*
4. Linear Dichroism and Optical Anisotropy of Silver Nanoprism Polymer Films 2016
   *Requena S, **Doan H**, Raut S, D'Achille A, Gryczynski Z, Gryczynski I, Strzhemechny YM. Nanotechnology. 2016 Jun 27;27(32):325704.*
5. Mechanothermal Control of the Conformation of a Porphyrin Dimer 2016
   ***Doan H**, Raut S, Yale D, Balaz M, Dzyuba SV, Gryczynski Z. Chemical Communications. 2016.*
6. Modifying optical properties of reduced/graphene oxide with controlled ozone and thermal treatment in aqueous suspensions 2016
   *Hasan, Md. Tanvir; Senger, Brian; Mulford, Price; Ryan, Conor; **Doan, Hung**; Gryczynski, Zygmunt (Karol); Naumov, Anton. Nanotechnology. 2016.*

Abstract

ATOTA – A VERY PROMISING GREEN FLUOROPHORE

By Hung The Doan, 2016

Department of Physics and Astronomy

Texas Christian University

Thesis Advisor:

Dr. Zygmunt K. Gryczynski, "Tex" Moncrief Jr. Chair Professor of Physics

Despite the fact that fluorescence community nowadays has invested in developing near-infrared probes, green fluorescence dyes like fluorescein and substitutes are still among the most widely used fluorophores for labeling in cellular imaging and biomedical research. Trioxatriangulenium dye $ATOTA^+$ is a very promising green fluorophore with high extinction coefficient and outstanding fluorescence quantum yield. This study focuses on characterizing $ATOTA^+$'s fundamental spectroscopic properties, including fluorescence and orientation of the transition moments. ATOTA's aggregation in aqueous solution and lipid bilayer membrane are also investigated. $ATOTA^+$ has absorption maxima between 470 nm and 476 nm and emission maxima between 496 nm and 511 nm depending on the solvent. The molar extinction coefficient varies from 135,000 $mol^{-1}cm^{-1}$ in nonpolar dichloromethane to above 90,000 $mol^{-1}cm^{-1}$ in polar solvents such as methanol. The quantum yield of $ATOTA^+$ is close to 1 in nonpolar DCM and decreases to 0.44 in polar DMF. $ATOTA^+$'s fluorescence lifetimes vary between 3.25 ns in aprotic low polarity triacetin to 1.66 ns in polar DMF. Furthermore, both radiative and non-radiative rates

are affected by solvent polarity. $ATOTA^+$ has very low water solubility due to the presence of 6 diethyl substitutions, and forms H-aggregates with a blue-shifted absorption maxima around 450 nm and red-shifted emission maxima of 580 nm respectively with fluorescence lifetime above 20 ns. The excitation anisotropy approaches 0.35 at red edge of the absorption spectrum and shape of polarization spectrum suggests the presence of overlapping transition moments in a S_0-S_1 band which is confirmed by linear dichroism in stretched PVA film. In DMPC lipid vesicles, $ATOTA^+$ forms a tight ion pair with a counter anion and localizes in the hydrocarbon interior. Overall we conclude that $ATOTA^+$ will be a highly useful and superior member of the green fluorophore family.